Reciprocal changes of H3K27ac and H3K27me3 at the promoter regions of the critical genes for endometrial decidualization

Running title: Epigenome analysis for endometrial decidualization

Abstract

Aim: Decidualization is essential for embryo implantation and placental development. We aimed to obtain transcriptome and epigenome profiles for primary endometrial stromal cells (ESCs) and *in vitro* decidualized cells

Materials & Methods: ESCs isolated from human endometrial tissues remained untreated (D0), or decidualized for 4 days (D4) and 8 days (D8) in the presence of 8-bromo-cAMP and progesterone.

Results: Among the epigenetic modifications examined (DNA methylation, H3K27ac, H3K9me3, and H3K27me3), the H3K27ac patterns changed most dramatically, with a moderate correlation with gene expression changes, upon decidualization. Subsets of up- and down-regulated genes upon decidualization were associated with reciprocal changes of H3K27ac and H3K27me3 modifications at their promoter region, and were enriched with genes essential for decidualization such as *WNT4*, *ZBTB16*, *PROK1*, and *GREB1*.

Conclusion: Our dataset is useful to further elucidate the molecular mechanisms underlying decidualization.

(136 words)

Summary Points

- Decidualization, the transformation of endometrial stromal cells (ESCs) into secretory decidual cells, is essential for successful implantation and pregnancy, and is dependent on the postovulatory increases in progesterone and local cyclic AMP production levels in humans.
- Although the responsiveness of ESCs to the hormonal cues is has been considered to be potentiated by genome-wide chromatin remodeling followed by the coordinated action of decidua-specific transcriptional networks, information for such epigenetic alterations has been limited.
- Through characterizing transcriptome and epigenome profiles for endometrial stromal cells and decidualized cells, we revealed that subsets of up- and down-regulated genes upon decidualization were associated with reciprocal changes of H3K27ac and H3K27me3 modifications at their promoter region.
- Among such genes, the top 23 genes, most extremely up-regulated, contained *WNT4*, *ZBTB16*, *PROK1*, and *GREB1*, shown to be essential for decidualization, and the top 8 genes, most extremely down-regulated, contained *CRABP2* and *PTHLH*, whose down-regulation has been shown to be critical for decidualization.
- Systematic functional characterization of the genes with reciprocal changes of H3K27ac and H3K27me3 modifications at their promoter region catalogued in this study is expected to uncover additional critical genes for decidualization, and to deepen our understanding of its molecular mechanisms.
- The epigenomic and transcriptomic profiles obtained in this study serve as high-quality data resources useful for searching cis/trans elements critical for decidualization, such as enhancers, transcription factors, non-coding RNAs, and their interactions to gene promoters.
- Integration of the epigenomic profiles for ESCs and decidualized cells with the genetic variant information relevant to endometrial disorders is expected to facilitate understanding molecular mechanisms underlying disease susceptibility.

Introduction

Endometrium, the inner layer of uterus, is essential for successful conception. It undergoes a cycle of regeneration, proliferation, differentiation and desquamation several hundred times during the reproductive age under the control of the ovarian steroidal hormones **[1,2]**. These dynamic morphological and functional changes during the menstrual cycle are thought to be epigenetically regulated. Endometrium is mainly composed of fibroblastic stromal and glandular epithelial cells. Decidualization, the transformation of endometrial stromal cells (ESC) into secretory decidual cells, is essential for embryo implantation and placental development, and is dependent on the postovulatory increase of progesterone and local cyclic AMP production levels in humans **[2,3]**. Defective decidualization has been implicated with spontaneous miscarriages **[4,5]**, preeclampsia **[6,7]**, and endometriosis **[8-10]**. Further delineation of molecular mechanisms operating decidualization is fundamental to develop therapeutic methodologies for these pathogenic conditions.

ESCs can be readily isolated from endometrium tissue and cultured. In the presence a mixture of ovarian hormones such as progesterone and estrogen, the cells undergo morphologic and biochemical changes and acquire characteristics of decidual cells **[11]**. These decidualized cells, *in vitro* model of decidualization, have been widely used to examine molecular mechanisms underlying decidual transformation **[1]**.

Epigenetic regulation of gene expression is essential for development and cellular differentiation **[12,13]**. The responsiveness of ESCs to the hormonal cues is considered to be potentiated by genome-wide chromatin remodeling followed by the coordinated action of decidua-specific transcriptional networks **[14-16].** Decidualization marker genes, *PRL* and *IGFBP1*, are known to be associated with epigenetics changes at their promoter regions, increased levels of H3K27ac (an active chromatin mark) and decreased levels of H3K27me3 (a repressive chromatin mark) **[17-19].**

Genome-wide histone modification patterns of ESCs and decidualized cells have been analyzed by two studies. One study **[17]** characterized the changes of H3K27me3 patterns between ESCs and decidualized cells at gene promoter regions by chromatin immunoprecipitation (ChIP) coupled with DNA microarray analysis, and identified

3,008 genomic regions including the IGFBP1 promoter region as regions showing a significant change of H3K27me3. Another study **[20]** investigated genome-wide changes in four types of histone modifications (H3K4me3, H3K27ac, and H3K4me1 as active marks and H3K27me3 as an inactive mark) associated with decidualization in ESCs using ChIP with next generation sequencing (ChIP-seq). The latter study demonstrated that the main changes in histone modifications upon decidualization are increases of H3K27ac and H3K4me3 at proximal and distal promoter regions, and identified only two and five regions as those with increased and decreased H3K27me3 signals, respectively, from genomic regions between - 10 kb and + 10 kb from transcription start sites (TSS) of the genes **[20]**.

In this study, to further capture the epigenetic dynamics and to understand its roles during decidualization, we conducted transcriptome and epigenome profiling for ESCs and decidualized cells. Epigenetic modifications we investigated include DNA methylation and three histone modifications, H3K27ac, H3K27me3, and H3K9me3 (a repressive chromatin mark). We confirmed relatively limited changes of repressive epigenetic modifications and the striking changes of H3K27ac levels correlated with gene expression changes in decidualization. We also revealed contribution of H3K27me3 changes at the promoter region of a portion of genes that are drastically up- and down-regulated upon decidualization. As far as we are aware of, ChIPseq data for H3K9me3 have been obtained for human ESCs and decidualized cells for the first time. We did not observe H3K9me3 changes at the promoters of up- and down-regulated gens upon decidualization.

Materials and Methods

Ethics

Donors of endometrial tissues provided written informed consent prior to endometrial tissue biopsy which was conducted in accordance with a protocol approved by the Institutional Review Boards at Juntendo University and the National Center for Child Health and Development.

Cell culture

Endometrial biopsies were obtained using the Pipelle Curette (CooperSurgical) from the uterine fundus from women of reproductive age without endometriosis who underwent laparoscopic cystectomy due to ovarian cyst. Characteristics of donor individuals are provided as **Table S1**. Endometrial stromal cells (ESCs) were isolated as reported previously **[21]** from endometrial tissues. After enzymatic digestion of minced tissues with 200 μg/ml collagenase B4 (SERVA, Heidelberg, Germany) in a shaking incubator for 2 hours at 37°C, cells were separated by filtration through a 40 μm nylon mesh. The dispersed fragments were collected by centrifugation, resuspended in MF-start medium and seeded on culture dishes. The residual tissue fragments and cell clumps were collected into a new 50ml tube using Accumax (Innovative Cell Technologies, San Diego, CA, USA) and 0.25% Trypsin/EDTA (Gibco, catalog no.25200-056, Thermo Fisher Scientific, Grand Island, NY, USA) and then incubated for 10 min at room temperature with continues pipetting. Cells separated by filtration through a 40 μm nylon mesh were collected by centrifugation, seeded in tissue culture dishes and incubated in phenol red-free DMEM containing glutamine, antibiotics, and 10% dextran-coated charcoal-stripped fetal bovine serum (FBS) at 37°C, 95% air and 5% CO2. ESCs were passaged serially (three times) until they reached to ten 10cm dishes with 80% confluency. ESCs in a 10cm dish were collected and subjected to immunostaining using fluorescently labelled anti-CD13 antibody followed by flow cytometry analysis to determine the percentage of the CD13-positive cells. ESCs in 9 dishes were divide into three groups (three each dishes) to obtain decidualized cells (D4 and D8) and control D0 cells. D8 cells were cultured in the differentiation medium, which contains 1 μM MPA

(Medroxyprogesterone 17 acetate, Sigma), 0.5mM 8-Br-cAMP (Sigma), 2% charcoal-stripped FBS in DMEM/F12 medium (life technologies), for 8 days for decidualization. D4 cells were cultured in the cell maintenance medium, DMEM/F12 medium supplemented with 2% charcoal-stripped FBS for 4 days, and in the differentiation medium for the subsequent 4 days. D0 cells were cultured in the cell maintenance medium for 8 days (**Fig.1A**). Medium was changed every other day for all types of cells in the 8-day culture period.

Nucleic acid isolation and quantitative RT-PCR

For each of three cell types (D0, D4, and D8), cells in one dish and two dishes were subjected to nucleic acid extraction and chromatin isolation, respectively. Genomic DNA and total RNA were isolated from cells using AllPrep DNA/RNA Kit (Qiagen). Quantitative RT-PCR was performed as described previously **[22]** using the following PCR primers: 5'-AAGCTGTAGAGATTGAGGAGCAAAC-3' and 5'-AAGCTGTAGAGATTGAGGAGCAAAC-3' for *PRL*, 5'- CGAAGGCTCTCCATGTCACCA-3' and 5'-TGTCTCCTGTGCCTTGGCTAAAC-3' for *IGFBP1*, and 5'- GCGGAAGGGTACAGCCAAT-3' and 5'-GCAGCCGGCGCAAA -3' for *L19*. The expression levels of *IGFBP1* and PRL normalized by that of *L19*.

RNA-sequencing and data analysis

Libraries for RNA-sequencing (RNA-seq) were prepared using NEBNext rRNA Depletion Kit (NEB #E6318) and NEBNext Ultra Directional RNA Library Prep Kit (NEB # E7420S) from 750ng of total RNA was a starting material. Paired end reads (101bp x2) obtained by the HiSeq2500 platform (Illumina) were trimmed for adapter sequences using cutadapt-1.7.1 and for low-quality bases at ends using a custom script, and mapped to the human reference genome (hg19) by Tophat2.1.1 (http://ccb.jhu.edu/software/tophat/index.shtml). After the removal of PCR duplicates using picard-tools-1.109, the resultant bam files were subjected to transcript assembly and quantification using Cufflinks 2.2.1 (http://cole-trapnell-lab.github.io/cufflinks/) with a gene annotation file (.gtf file) obtained from Illumina iGenomes website

(https://support.illumina.com/sequencing/sequencing_software/igenome.html) (archive-2012-03-09-03-24-41). Gene expression values were calculated as fragments per kilobase of exon per million mapped fragments (FPKM). FPKM values smaller than 0.3 were regarded as "not expressed" and transformed to 0.3. Gene Ontology (GO) analysis was performed using the Database for Annotation, Visualization and Integrated Discovery (DAVID) (https://david.ncifcrf.gov/) using the official gene symbols of differentially expressed RefSeq genes extracted from the genes_fpkm.tracking file (Cuffdiff output). FPKM values and positional information of TSSs from the tss_fpkm.tracking file (Cuffdiff output) were used for integrative analyses of transcriptome and histone modification profiles.

DNA methylation profiling

Genome-wide DNA methylation profiles of endometrial stromal (D0) and decidualized cells (D4 and D8) were obtained using an Illumina Infinium HumanMetylation 450 BeadChip as described previously **[23]**. The image data obtained using an iScan system (Illumina) were processed with the GenomeStudio software (Methylation Analysis Module version 1.9.0, Illumina) with background subtraction and control normalization options. Methylation levels for each of over 480,000 CpG sites were calculated as a β value (= intensity of the methylated allele/[intensity of the unmethylated allele + intensity of the methylated allele + 100]), ranging from 0 (completely unmethylated) to 1 (completely methylated). Probes with a missing β value or a high detection p-value (>0.01) were excluded for further analysis.

Chromatin immunoprecipitation

Cells were collected from three 10 cm dishes, cross-linked with 1% formaldehyde for 10 min at 37°C, and 2M glycine solution was added to the cell suspension (final concentration 0.125 M). The fixed cells were resuspended in SDS lysis buffer (ChIP Reagent, Nippon Gene Co., Ltd.) and the lysate was sonicated to fragment chromatin using a S220 Focused-ultrasonicator (Covaris). The chromatin was purified by centrifugation and

159 immunoprecipitated with Dynabeads M-280 sheep anti-mouse IgG (Veritas Life Sciences) conjugated to mouse
160 IgG (Abcam: ab37415), anti-H3K9me3 antibodies (CMA318), anti-H3K27me3 (CMA323), or anti-H3K27ac
161 (CMA309) in 1xRIPA (150mM) buffer with protease inhibitor (ChIP Reagent) 4-6 h at 4 °C. The chromatin bound
162 with beads were washed 1xRIPA (150 mM) buffer, 1xRIPA (500 mM) buffer and TE buffer. After washing, the
163 chromatin bound with beads were incubated in ChIP direct elution buffer (ChIP Reagent) for overnight at 65 °C
164 (for reverse cross-linking), followed by the incubation with proteinase K for 2 h at 55 °C. The DNA
165 immunoprecipitated from the supernatant was purified using AMPure XP beads (Beckman Coulter) according to
166 the manufacturer's instructions.
167
168 ***ChIP sequencing (ChIP-seq) and data analysis***
169 ChIP-seq and input libraries were prepared from 0.1 to 1.0 ng of ChIP DNA samples (from D0, D4, and D8 cells)
170 and 1.0ng of input DNA samples (from D4 cells), respectively, using NEBNext Ultra II DNA Library Prep Kit for
171 Illumina (NEB, E7645S). Single end reads (51bp) were obtained by the HiSeq2500 platform (Illumina). Reads
172 from each of ChIP-seq and input libraries were first trimmed for adapter sequences using cutadapt-1.7.1 and for
173 low-quality bases at ends using a custom script, and aligned to the human reference genome (hg19) using the
174 Burrows-Wheeler Aligner 0.6.2 (http://bio-bwa.sourceforge.net/). PCR duplicates were removed using picard-
175 tools-2.8.1 (http://broadinstitute.github.io/picard/). The resultant bam files (including multi-hit reads) of the pairs
176 of ChIP and input libraries were subjected to peak detection using MACS2 (https://github.com/taoliu/MACS) with
177 the broad peak calling option for H3K27me3 and H3K9me3. For further analyses of H3K27ac peaks, genomic
178 regions of peaks in bed format detected in six samples (D0, D4, and D8 cells of EM0409 and EM0519) were
179 merged as one bed file using the *merge* command of bedtools2.26.0 (http://bedtools.readthedocs.io/en/latest/).
180 Mapped reads of H3K27ac ChIP-seq libraries and input libraries were counted for each of merged peaks using
181 the *annotate* command of bedtools2.26.0. For further analyses of H3K9me3 and H3K27me3 data, mapped reads
182 of all ChIP and input libraries and were counted for each of 1000-bp windows of the hg19 reference genome with

183 the *annotate* command of bedtools2.26.0. Windows whose maximal count among three samples (D0, D4, D8) is
184 smaller than 20 were removed for further analyses. Read counts for peak regions (H3K27ac and input data) and
185 1,000-bp windows (H3K9me3, H3K27me3, and input data) were counted. ChIP read counts were divided by the
186 input read counts of the corresponding peak region or window. The resultant enrichment scores were subjected
187 to quantile normalization using the normalizeQuantiles function in the limma package of R (https://www.r-
188 project.org/). The quantile-normalized enrichment scores of H3K27ac and H3K27me3 for the 2,000 upstream
189 regions of RefSeq TSSs were calculated in the same manner.
190 MACS2, seqMINER (https://github.com/zhanxw/seqminer), *ngs.plot* (https://github.com/shenlab-sinai/ngsplot)
191 and custom R scripts were used to analyze ChIP-seq data. Integrative Genomics Viewer (IGV,
192 http://software.broadinstitute.org/software/igv/) was used to visualize ChIP-seq peaks together with RNA-seq
193 data.

Results

Transcriptome and epigenome profiling for ESCs and decidualized cells

We obtained ESCs and decidualized cells (D4 and D8) through the cell culture conditions shown in **Fig.1A** from two donor individuals (EM0409 and EM0519). The percentage of CD13-positive cells among the isolated ESCs determined by immune-staining followed by flow cytometry analysis was > 85% (data not shown). The differentiation status of the cells was confirmed by quantitative RT-PCR for two decidualization marker genes, *PRL* and *IGFBP1* **[2]**. Both genes were dramatically up-regulated (839 ~ 39,743 folds) in D4 and D8 cells as expected (**Fig.1B**). We subsequently obtained transcriptome and methylome profiles, and histone modification (HM) profiles for H3K27ac (an active chromatin mark), and for H3K9me3 and H3K27me3 (repressive chromatin marks). We obtained high quality data for the majority (99.6%) of 482,421 CpG loci that are covered by the HumanMethylation450 BeadChip array platform. We mapped sequence reads obtained from RNA-seq and ChIP-seq libraries to the hg19 human reference genome as described in **the Materials and Methods**, and examined the library metrics such as mapping and PCR duplicate rates to confirm their data quality (**Table S2**). We also assessed the quality of ChIP-seq data by visual inspection of peak shapes using IGV (http://software.broadinstitute.org/software/igv/) and peak calling results using MACS2 (https://github.com/taoliu/MACS) (**Table S2**). We subjected all transcriptome and epigenomic profiles to the subsequent data analyses except for one, the H3K27ac profile of EM0519_D8 cells due to its low peak numbers.

Gene expression changes upon decidualization

We counted the numbers of differentially expressed genes upon decidualization. Among the 14,962 RefSeq genes that were expressed (FPKM > 0.3) in at least one of the six samples (D0, D4, and D8 cells from two donors), 1,646 (10.9%) and 2,055 (13.6%) genes were commonly up-regulated (FPKM fold-change >2.0) in D4 and D8 compared to D0, and 712 (4.7%) and 905 (6.0%) genes were commonly down-regulated (fold-change < 0.5) (**Fig.1C, Table S3**). We compared our data with those of a previous microarray-based expression study for

decidualization **[24]**, and confirmed that 45 out of top 50 up-regulated and 34 out of top 50 down-regulated genes reported by Takano *et al.* **[24]** were also found to be differentially expressed in our study. Gene ontology analysis using DAVID 6.7 (https://david-d.ncifcrf.gov/) detected several each of statistically significantly enriched GO terms among both up-regulated and down-regulated genes (**Fig.1D**, **Table S4**). The detected GO terms include those recapitulating the well-defined features of decidualization **[2]**, such as up-regulation of genes involved in "cholesterol biosynthetic process" (for steroid hormone production), down-regulation of genes involved in "DNA replication" (for cell cycle arrest), and up- and down-regulation of genes involved in "extracellular matrix organization". The consistency of GE patterns upon decidualization between this and previous studies assures the suitability of the *in vitro* differentiated cells obtained in this study for epigenomic profiling.

Limited DNA methylation changes upon decidualization

We obtained DNA methylation profiles for 480,825 CpG sites of cells from the donor EM0409. When methylation β value differences ($\Delta\ \beta$) > 0.2 and < -0.2 were considered as differentially methylated, only 18 (0.004%) and 337 (0.07%) CpG sites were hyper- and hypo-methylated in decidualized (D8) cells compared to control D0 cells, respectively (**Fig 2A**). DNA methylation profiles of the cells from the donor EM0519 also showed similar methylation patterns (data not shown). These results indicate that the majority of the GE changes observed upon decidualization (**Fig.1C, Fig.2B**) are independent of CpG methylation alterations.

Histone modification profiles of ESCs and decidualized cells

We initially assessed the extents of reproducibility between two biological replicates and of differences upon decidualization for GE and HM profiles (**Fig.2B**). The scatter plots represent comparisons of normalized enrichment scores (calculated as described in **the Materials and Methods**) for 64,497 merged peaks for H3K27ac, 1,280,496 windows for H3K27me3, and 920,113 windows for H3K9me3 (window size: 1,000 bp). Pearson correlation coefficients of the comparisons between biological replicates (boxed in blue) for HMs ranged

from 0.68 (D4, H3K9me3) to 0.89 (D0, H3K27ac), demonstrating overall high reproducibility. In the comparisons among D0, D4, and D8 cells from the same donor, the distributions of mapped read counts per window were highly correlated for H3K9me3 and H3K27me3, with correlation coefficients between 0.80 and 0.86. In contrast, the distributions of mapped read counts per peak for H3K27ac were different between control D0 cells and decidualized (D4, D8) cells, with correlation coefficients between 0.20 and 0.36. When differential enrichment thresholds of fold-change > 2 and fold-change <0.5 were used for increase and decrease upon decidualization, the ratios of peaks or 1,000 bp windows that were differentially enriched in D4 compared to D0 in both series were 15.4% and 16.7% for H3K27ac peaks, 0.3% and 0.7% for H3K27me3 windows, and 0.3% and 0.3% for H3K9me3 (counts and ratios for individual sets are listed in **Table S5**). These results indicate that H3K27ac patterns change most dramatically upon decidualization among the three HMs examined.

Correlation of gene expression and histone modification changes in ESCs and decidualized cells

We subsequently examined the extent of correlation of GE changes and HM changes at gene promoter regions. Fold changes of FPKM values for TSSs in D4 relative to those in D0, and fold-changes of normalized enrichment scores of histone modifications in D4 relative to those in D0, were assessed for their correlation. Only TSSs whose FPKM values were greater than 0.3 in D0 or D4 were subjected to the analysis. When HM peaks or windows (**Table 1**) located within 2,000 bp distance from a TSS were assessed for EM0409 (**Fig.3A**), the Spearman correlation coefficients between GE changes and HM changes were 0.54 (H3K27ac), -0.22 (H3K27me3), and 0.16 (H3K9me3), suggesting a moderate positive correlation of H3K27ac levels and a weak negative correlation of H3K27me3 levels with GE changes. Similar results were obtained for EM0509 (**Table S6**). We also drew average profiles of three HMs along gene structure for four sub-categories of genes depending on their GE levels: no expression, FPKM =< 0.3; low, 0.3 < FPKM =< 1; middle, 1 < FPKM =< 10; high, FPKM > 10) (**Fig.3B**). In case of EM0409_D0 (22,493 genes in total), the ratios of four subcategories were 39.1% (no), 7.4% (low), 27.2% (middle), and 26.2% (high). H3K27ac levels at the TSS regions were proportional to GE levels, and

H3K27me3 and H3K9me3 levels were inversely related to GE levels at the promoter regions and gene bodies. These patterns are consistent with well-established features of H3K27ac being an active promoter mark and H3K27me3/H3K9me3 being repressive marks. The other five ESC and decidualized cells showed highly similar patterns with those of EM0409_D0 (**data not shown**).

To delineate HM changes along the genes with GE alterations upon decidualization, we drew average profiles of HMs for 506 and 349 genes that were up- (fold change > 4) and down-regulated (fold change < 0.25) in D4 cells compared to D0 cells (**Fig.3C, Fig.S1**). For between-sample comparisons of HM profiles, we normalized their reads per million values (determined by *ngs.plot*) by the ratio of the median of quantile-normalized enrichment scores to the median of enrichment scores before quantile-normalization. The average H3K27ac levels at the TSS regions became higher among up-regulated genes and lower among down-regulated genes in D4 and D8 cells compared to D0 cells. The average H3K27me3 level among up-regulated genes became noticeably lower in D4 than in D0 cells, suggesting the possibility that gain of H3K27ac and loss of H3K27me3 occurred simultaneously at a subset of the up-regulated promoter regions. Such reciprocal changes have been previously described at the promoters of decidualization marker genes, *IGFBP1* and *PRL* **[17-19]**.

Selection of up- and down-regulated gene promoters upon decidualization accompanied with reciprocal changes of H3K27ac and H3K27me3 levels

Reciprocal changes of H3K27ac and H3K27me3 modifications at a gene promoter are expected to be associated with a drastic change in GE levels: the tight repression in ESCs and highly elevated expression upon decidualization (or *vice versa*). We obtained quantile-normalized enrichment scores of H3K27ac and H3k27me3 in 2,000 bp upstream regions of 21,753 RefSeq TSSs as described in **the Materials and Methods,** and selected the following TSS sets: 664 TSSs with H3K27ac enrichment score (27ac_ES) >= 2 and H3K27me3 ES (27me3_ES) >= 0.5 as those accompanied with H3K27ac increase only (orange), 306 TSSs with 27ac_ES >= 2 and 27me3_ES < 0.5 as those accompanied with H3K27ac increase and H3K27me3 decrease (red), 816 TSSs

with 27ac_ES < 0.5 and 27me3_ES < 2 as those accompanied with H3K27ac decrease only (light blue), and 220 TSSs with 27ac_ES < 0.5 and 27me3_ES >= 2 as those accompanied with H3K27ac decrease and H3k27me3 increase (blue). The extents of expression fold-changes of genes associated with reciprocal HM changes (red and blue) tended to be larger than those of genes associated with H3K27ac change alone (orange and light blue) at the promoter regions (**Fig.4A and B**) with statistical significance (**Fig.S2**). Scatter plot representation of FPKM values of those genes in D0 and D4 cells (**Fig.4B**) also demonstrated the presence of a subset of genes that are tightly repressed in one cell type and highly expressed in the other.

We hypothesized that genes whose promoter exhibits reciprocal alterations of H3K27ac and H3K27me3 upon decidualization are enriched with those having essential functions in decidualization, and searched for such promoters. The numbers of the H3K27ac peaks and H3K27me3 whose enrichment levels were higher (fold-change > 2) and lower (fold-change < 0.5) in D4 compared to D0 commonly in two series (EM0409 and EM0519) were 9,951 and 9,384, respectively (**Table S6**). The center base position of the overlapped regions of the H3K27ac peaks of EM0409_D4 and EM0519_D4 was padded with 2,000 bp on both sides. Among the resultant 4,000 bp intervals, 4,548 had an overlap (>=1 bp) with an H3K27me3-decreased window. Among those H3K27ac-increased/H3K27me3-decreased regions, 1,304 regions were flanked by a TSS located within 5000 bp distance. Among those, 572 regions whose associated gene was up-regulated (fold-change > 2) in D4 compared to D0 in both EM0409 and EM0519 were selected as candidates. We visually inspected the HM patterns of a portion of these 572 candidates using IGV, and realized that regions with low levels of H3K27me3 in D0 cells and regions with low levels of H3K27ac in D4 cells were included among them. Therefore, we excluded the regions with the H3K27me3 enrichment score less than the 10th percentile value in D0 cells and the regions with the H3K27ac enrichment score less than the 10th percentile value in D4 cells. The resultant 417 regions were regarded as candidates for up-regulated promoters with the increase of H3K27ac and the decrease of H3K27me3 marks. Similarly, among the 10,788 regions whose H3K27ac level decreased (fold change < 0.5) commonly in EM0409 and EM0519, 249 regions had an overlap with one of the 3,790 regions whose H3K27me3 level increased (fold-

change > 2) commonly. Among those, 75 regions, being flanked by a TSS of the down-regulated (fold-change < 0.5) genes within 5,000 bp distance, were selected as candidates for down-regulated promoters with the decrease of H3K27ac and the increase of H3K27me3 marks. It should be also noted that the padded 4,000 bp intervals of H3K27ac-increased or -decreased regions were partially overlapped each other when multiple H3K27ac peaks existed within a 2000 bp interval. After eliminating such redundantly counted regions, we identified 125 up-regulated and 45 down-regulated RefSeq gene promoters that are accompanied with reciprocal changes of H3K27ac and H3K27me3 modifications upon decidualization (**Table S8**). Among those, 23 up-regulated and 8 down-regulated promoters were further selected as those fulfilling the FPKM log2 fold-change criteria of > 4 or < -4, and are shown in **Fig.4C.** The H3K27ac, H3K27me3, and RNA-seq profiles in D0, D4, and D8 cells of EM0409 visualized using IGV are shown for six loci in **Fig.4D**. *PRL* and *IGFBP1* represent loci previously reported to be associated with reciprocal changes of H3K27ac and H3K27me3 **[17-19].** While the decrease of the H3K27me3 levels in D4 cells compared to those in D0 cells was visually discernible at the promoter regions of the *PRL* and *IGFBP1 genes* (**Fig.4D**), those regions fell slightly short of our selection criteria described above. The other four loci, *WNT4*, *ZBTB16*, *HSD11B1*, and *ADRA2A,* were selected as examples of the loci that fulfilled our criteria (**Fig.4C**, **Table S8**).

Discussion

We successfully obtained genome-wide histone modification profiles of H3K27ac, H3K27me3, and H3K9me3 for human ESCs and decidualized cells by ChIP-seq analysis. The H3K9me3 profiles were obtained for these cells for the first time. The roles of these three histone modifications have been very well established by a large number of past studies including consortium projects **[25]**. H3K27ac marks active promoters and enhancers, and therefore represents an indicator of gene expression **[25]**. H3K27me3 and H3K9me3 are repressive marks associated with polycomb repression and heterochromatin, respectively **[25]**. Consistently, we observed a positive correlation between GE changes and H3K27ac changes at promoter regions and a weak negative correlation between GE changes and H3K27me3 changes at promoter regions (**Fig.3A**).

Although the H3K27ac and H3K27me3 profiles have already been reported previously **[17,20]**, our data for these histone modifications enabled us to have detected larger numbers of peaks and differentially enriched regions upon decidualization. For instance, whereas Tamura *et al* **[20]** reported the numbers of H3K27ac-increased and -decreased regions upon decidualization to be 3,705 and 42, respectively, we detected 9,951 and 10,788 regions as H3K27ac-increased and -decreased regions upon decidualization (**Table S5**). The high correlation coefficients (0.89 and 0.77) of the mapped read counts per peak of the H3K27ac profiles of the biological replicates (**Fig.2B**) demonstrate the reliability of our dataset. Whereas we and Grimaldi *et al* **[17]** detected thousands of H3K27me3-increased and -decreased regions upon decidualization, Tamura *et al* **[20]** detected less than ten of such regions. The authors mentioned the possibility that the differences in the reagents and the culture duration to induce decidualization may underlie the discrepant results between the two studies, Grimaldi *et al.* and Tamura *et al.* **[20]**. According to suggestions during the review procedure, we re-analyzed ChIP-seq data by Tamura *et al.* **[20]** using our bioinformatic protocols described in **the Materials and Methods**, and detected peaks using MACS2 (**Table S2**). The numbers of H3K27ac peaks detected for four samples were 9071, 2677, 18764, and 497. The

number of H3K27me3 peaks detected with the broad option of MACS2 was zero for all four samples. These low peak numbers indicate overall low signal-to-noise ratios of ChIP-seq data by Tamura *et al.*

There are many bioinformatic tools available to detect differential regions for histone modification enrichment. A recent comprehensive comparison of 14 tools for differential ChIP-seq analysis **[26]** has revealed that these tools show a great variety in the type of signal detected with a low level of agreement, and therefore warned that the choice of the differential peak detection tools will crucially impact the outcome. These tools are diverse in many critical points such as the method of normalization and statistical test, requirement for prior peak detection by external algorithms and biological replicates, and the types of peaks (sharp, broad or both) for which the tool was designed. In this study, for differential peak detection for H3K27me3 and H3K9me3, we did not use the existing differential ChIP-seq analysis tools and analyzed normalized read counts (per 1,000 bp window) obtained using bedtools, R and custom shell scripts. We preferred our own analysis than the existing tools because the majority of them were not compatible with our data after quantile normalization. For the differential peak detection for H3K27me3 and H3K9me3, we applied the window size (1,000 bp) used in Tamura *et al* **[20]**, and did not examine the effects of window sizes on the differential peak detection.

In this study, we first observed that H3K27ac patterns changed most dramatically upon decidualization, and were correlated with GE changes. Subsequently, we noticed that, although the alterations of the repressive histone modifications (H3K9me3 and H3K27me3) were much more limited than those of H3K27ac, the average level of H3K27me3 associated with up-regulated genes upon decidualization became lower in decidualized cells (D4 and D8) than ESCs (D0) (**Fig.3C**). These observations led us to search for gene promoter regions whose up- and down-regulation upon decidualization is associated with reciprocal changes of H3K27ac and H3K27me3. Genes driven by such promoters were expected to be tightly repressed in ESCs and to get drastically up-regulated in a manner dependent of cAMP and progesterone actions, or vice versa. We observed such a tendency especially in the genes up-regulated upon decidualization (**Fig.4A**, **Fig.S2** and **Table S9**). Importantly, the 90 genes up-

374 regulated upon decidualization with reciprocal changes of H3K27ac and H3K27me3 at their promoter (**Fig.4C**
375 and **Table S8**) include at least four genes that have been shown to be functionally essential for decidualization,
376 namely, *WNT4* **[27]**, *ZBTB16* **[28]**, *PROK1* **[29]**, and *GREB1* **[30]**. siRNA knockdown of these genes has been
377 shown to inhibit steroid hormone-induced decidualization of human ESCs **[27-30]**. Because the majority of 90
378 genes has not been tested for their roles in decidualization, systematic functional characterization of these genes
379 (e.g., siRNA knockdown screening) is effective for identifying additional critical genes for decidualization, and to
380 deepen our understanding of its molecular mechanisms.
381 The 90 up-regulated genes (**Fig.4C**, **Table S8A**) also contain genes known to be critical for decidualization and
382 its functions (such as *HSD11B1*, *CNR1*, and *EDNRB*) and genes potentially possessing as-yet-unknown
383 important functions in decidualization such as *SCARA5*. The progesterone-dependent induction of *HSD11B1*
384 encoding hydroxysteroid 11-beta dehydrogenase 1 leads to cortisol biosynthesis in decidualized cells and
385 transcriptional regulation of glucocorticoid receptor and mineralocorticoid receptor-mediated gene networks **[31]**.
386 *CNR1* encodes cannabinoid receptor I. Endocannabinoid signaling is proposed to modulate decidualization **[32]**,
387 and to be critical in regulating decidual senescence and parturition timing **[33,34]**. *EDNRB* encodes endothelin
388 receptor B, which binds members of the endothelin family proteins that regulate endometrial blood flow **[35]**.
389 EDNRB has been proposed as a factor involved in endometrial receptivity **[36]**, a temporally unique sequence of
390 factors that make the endometrium receptive to embryonic implantation **[37]**. *SCARA5* is known to encode a
391 ferritin receptor mediating non-transferrin iron delivery **[38]**. The observed expression pattern of this gene, tight
392 suppression in ESCs and high expression in decidualized cells, suggests an unknown role of ferritin-mediated
393 regulation in decidualization.
394 Grimaldi *et al*. **[17]** has shown by ChIP-qPCR that the H3K27me3 levels near the TSS of the *PRL* and *IGFBP1*
395 genes decreased to approximately 40% and 25% levels four days after induction of decidualization compared to
396 the levels before induction of decidualization, and decreased to further lower levels (less than 10 % and 5%,
397 respectively) eight days after induction of decidualization. In addition to the drastic increase of H3K27ac levels at

398 the promoter regions of *PRL* and *IGFBP1* genes, we observed the decrease of H3K27me3 levels at these
399 promoter regions upon decidualization as shown in **Fig.4D**. However, the H3K27me3 levels of the *PRL* promoter
400 region in D0 cells were not higher than the selection criterion applied. The fold-change decrease of the H3K27me3
401 level at the *IGFBP1* promoter in D4 cells compared to D0 cells satisfied our criterion (fold-change < 0.5) in the
402 cells derived from EM0409, but no in the cells derived from EM0519.

403 The 38 down-regulated genes upon decidualization with reciprocal changes of H3K27ac and H3K27me3 at their
404 promoter also contain genes whose appropriate expression is critical for decidualization. Coculture of endometrial
405 cells overexpressing *CRABP2* with trophoblast spheroids has been reported to impair spheroid expansion **[39]**.
406 Parathyroid hormone-like hormone encoded by the *PTHLH* gene has been shown to represses decidualization
407 of human uterine fibroblast cells **[40]**. These previous studies support the functional importance of down-
408 regulation of *CRABP2* **[41]** and *PTHLH* upon decidualization for successful pregnancy. Functional
409 characterization of the other down-regulated genes such as *ADRA2A* (encoding Adrenoceptor Alpha 2A) and
410 *WNT2* may lead to identify novel signaling pathways or further fine-tuning mechanisms of known signaling
411 pathways essential for decidualization.

412 Array-based DNA methylation profiling of approximately 48 thousand CpG sites for ESCs (D0) and decidualized
413 cells (D4 and D8) revealed that the alterations of DNA methylation upon decidualization are very limited (**Fig.2A**),
414 consistent with a previous report **[42]**. This result does not exclude the possibility of the significant role of DNA
415 methylation at specific loci that may not be covered by the DNA methylation array platform adopted in this study.
416 Interestingly, Lucas *et al* **[43]** recently reported a possible involvement of non-CpG DNA methylation in
417 endometrial decidualization. However, the array-based method utilized in this study is not designed to measure
418 non-CpG methylation in a genome-wide manner. Therefore, it is important to further accumulate sequencing-
419 based whole genome methylome data for ESCs and decidualized cells to elucidate the role of DNA methylation
420 in the epigenetic regulation of decidualization and related diseases.

In the gene ontology analysis for differentially expressed genes upon decidualization, we detected the GO term "nucleosome assembly" as a term highly enriched among down-regulated genes (**Fig.1D**, **Table S3**) due to the presence of nearly 20 histone genes that express replication-dependent non-polyadenylated histone mRNAs. These histone genes were expressed in ESCs but were down-regulated in decidualized cells as they stopped cell divisions. We were able to detect these non-poly(A) transcripts in addition to poly(A) transcripts because we adopted a ribosomal RNA depletion protocol in RNA-seq library preparation. Detail analyses of our RNA-seq data may reveal unidentified roles of non-poly(A) non-coding RNAs in decidualization.

In this study, we successfully obtained genome-wide profiles of an active promoter/enhancer mark (H3K27ac) and repressive chromatin marks (H3K9me3 and H3K27me3) in ESCs and decidualized cells, and mainly focused on their dynamics at gene promoter regions. Our dataset, including RNA sequencing data, provides a foundation to further elucidate molecular mechanisms governing decidualization through identifying critical *cis*/*trans* elements such as enhancers, transcription factors, non-coding RNAs, and their interactions to promoters.

Although our study successfully obtained GE and three types of HM profiles for ESCs and decidualized cells showing sufficient reproducibility between two biological replicates, our study design has limitations in elucidating intrinsic and environmental factors that possibly affect the epigenomic status of the cells, such as patient history, phases of menstrual cycle from which the cells were originally isolated, and the cell culture conditions (passage numbers, types and concentrations of reagents to induce decidualization, and duration of their administration). Human genetic variations affect gene expression and disease susceptibility. Expression quantitative trait (eQTL) loci for endometrial gene expression have been identified as 18,595 cis expression regulatory SNPs for 198 genes recently **[44]**. Genome-wide association studies (GWAS) have identified 12 SNPs (at 10 independent loci) associated with associated with endometriosis **[45]**. Integration of the epigenomic profiles for ESCs and decidualized cells presented here with the datasets of the genetic variations relevant to the endometrial tissue

443 and its related diseases is expected to facilitate elucidating molecular mechanisms through which genetic variants
444 contribute to disease susceptibility. Our dataset (**Fig.S3**) serves as the reference for the future studies to examine
445 the effects of genetic variants on the epigenome of ESCs and decidualized cells and for the comparison with GE
446 and HM profiles obtained for ESCs and decidualized cells derived from the endometrial tissues of the patients
447 with endometrial disorders such as endometriosis, recurrent miscarriage, and implantation failure.

References

[1] Rock J, Bartlett MK. Biopsy studies of human endometrium: criteria of dating and information about amenorrhea, menorrhagia, and time of ovulation. ***J. Am. Med. Assoc.*** 108(24), 2022-2028 (1937).

[2] Gellersen B, Brosens JJ. Cyclic decidualization of the human endometrium in reproductive health and failure. ***Endocr. Rev.*** 35(6), 851-905 (2014).

** A comprehensive and enlightening review article covering a wide range of important topics for the decidualization of the human endometrium

[3] Gellersen B, Brosens J. Cyclic AMP and progesterone receptor cross-talk in human endometrium: a decidualizing affair. ***J. Endocrinol.*** 178(3), 357-372 (2003).

[4] Salker M, Teklenburg G, Molokhia M et al. Natural selection of human embryos: impaired decidualization of endometrium disables embryo-maternal interactions and causes recurrent pregnancy loss. ***PLoS One.*** 5(4), e10287 (2010).

[5] Brosens JJ, Salker MS, Teklenburg G et al. Uterine selection of human embryos at implantation. ***Sci. Rep.*** 4, 3894 (2014).

[6] Garrido-Gomez T, Dominguez F, Quiñonero A, Diaz-Gimeno P et al. Defective decidualization during and after severe preeclampsia reveals a possible maternal contribution to the etiology. ***Proc. Natl. Acad. Sci. U S A.*** 114(40), E8468-E8477 (2017).

[7] Conrad KP, Rabaglino MB, Post Uiterweer ED. Emerging role for dysregulated decidualization in the genesis of preeclampsia. ***Placenta*** 60,119-129 (2017).

[8] Aghajanova L, Horcajadas JA, Weeks JL et al. The protein kinase A pathway-regulated transcriptome of endometrial stromal fibroblasts reveals compromised differentiation and persistent proliferative potential in endometriosis. ***Endocrinology*** 151(3), 1341-1355 (2010).

[9] Klemmt PA, Carver JG, Kennedy SH et al. Stromal cells from endometriotic lesions and endometrium from women with endometriosis have reduced decidualization capacity. ***Fertil. Steril.*** 85(3), 564-572 (2006).

[10] Yin X, Pavone ME, Lu Z et al. Increased activation of the PI3K/AKT pathway compromises decidualization of stromal cells from endometriosis. ***Clin. Endocrinol. Metab.*** 97(1), E35-43 (2012).

[11] Tabanelli S, Tang B, Gurpide E. In vitro decidualization of human endometrial stromal cells. ***J. Steroid Biochem. Mol. Biol.*** 42(3-4), 337-344 (1992).

[12] Zhou VW, Goren A, Bernstein BE. Charting histone modifications and the functional organization of mammalian genomes. ***Nat. Rev. Genet.*** 12(1), 7-18 (2011).

[13] Creyghton MP, Cheng AW, Welstead GG et al. Histone H3K27ac separates active from poised enhancers and predicts developmental state. ***Proc. Natl. Acad. Sci. U S A.*** 107(50), 21931-21936 (2010).

[14] Munro SK, Farquhar CM, Mitchell MD et al. Epigenetic regulation of endometrium during the menstrual cycle. ***Mol. Hum. Reprod***. 16(5), 297-310 (2010).

[15] Garrido-Gomez T, Dominguez F, Lopez JA et al. Modeling human endometrial decidualization from the interaction between proteome and secretome. ***J. Clin Endocrinol Metab.*** 96(3), 706-716 (2011).

[16] Zelenko Z, Aghajanova L, Irwin JC et al. Nuclear receptor, coregulator signaling, and chromatin remodeling pathways suggest involvement of the epigenome in the steroid hormone response of endometrium and abnormalities in endometriosis. ***Reprod Sci.*** 19(2), 152-162 (2012).

[17] Grimaldi G, Christian M, Steel JH et al. Down-regulation of the histone methyltransferase EZH2 contributes to the epigenetic programming of decidualizing human endometrial stromal cells. ***Mol. Endocrinol.*** 25(11), 1892-1903 (2011).

** The paper represents the first study that obtained the genome-side histone modification profiles of H3K27me3 for ESCs and decidualized cells by chromatin immunoprecipitation (ChIP) coupled with DNA microarrays for gene promoter regions. The authors confirmed the decreased levels of H3K27me3 at the proximal promoter regions of the *PRL* and the *IGFBP1* genes upon decidualization by ChIP-qPCR.

[18] Tamura I, Asada H, Maekawa R et al. Induction of IGFBP-1 expression by cAMP is associated with histone acetylation status of the promoter region in human endometrial stromal cells. ***Endocrinology*** 153(11), 5612-5621 (2012).

[19] Tamura I, Sato S, Okada M et al. Importance of C/EBPβ binding and histone acetylation status in the promoter regions for induction of IGFBP-1, PRL, and Mn-SOD by cAMP in human endometrial stromal cells. ***Endocrinology*** 155(1), 275-286 (2014).

[20] Tamura I, Ohkawa Y, Sato T et al. Genome-wide analysis of histone modifications in human endometrial stromal cells. ***Mol. Endocrinol.*** 28(10), 1656-1669(2014).

[21] Masuda A, Katoh N, Nakabayashi K et al. An improved method for isolation of epithelial and stromal cells from the human endometrium. ***J. Reprod.*** 62(2), 213-218 (2016).

[22] Yoshida W, Tomikawa J, Inaki M et al. An insulator element located at the cyclin B1 interacting protein 1 gene locus is highly conserved among mammalian species. ***PLoS One*** 10(6), e0131204 (2015).

[23] Miyata T, Sonoda K, Tomikawa J et al. Genomic, Epigenomic, and Transcriptomic Profiling towards Identifying Omics Features and Specific Biomarkers That Distinguish Uterine Leiomyosarcoma and Leiomyoma at Molecular Levels. ***Sarcoma*** 412068 (2015).

[24] Takano M, Lu Z, Goto T et al. Transcriptional cross talk between the forkhead transcription factor forkhead box O1A and the progesterone receptor coordinates cell cycle regulation and differentiation in human endometrial stromal cells. ***Mol. Endocrinol.*** 21(10), 2334-2349 (2007).

[25] Roadmap Epigenomics Consortium, Kundaje A, Meuleman W et al. Integrative analysis of 111 reference human epigenomes. ***Nature*** 518(7539):317-330 (2015).

[26] Steinhauser S, Kurzawa N, Eils R, Herrmann C. A comprehensive comparison of tools for differential ChIP-seq analysis. ***Brief Bioinform***. 17(6):953-966. (2016).

[27] Li Q, Kannan A, Das A et al. WNT4 acts downstream of BMP2 and functions via β-catenin signaling pathway to regulate human endometrial stromal cell differentiation. ***Endocrinology*** 154(1), 446-457 (2013).

[28] Kommagani R, Szwarc MM, Vasquez YM et al. The Promyelocytic Leukemia Zinc Finger Transcription Factor Is Critical for Human Endometrial Stromal Cell Decidualization. ***PLoS Genet.*** 12(4), e1005937

(2016).

* By integrating genome-wide datasets for the decidualization of human ESCs, the authors identified the promyelocytic leukemia zinc finger (PLZF) transcription factor encoded by the *ZBTB16* gene as a critical factor for progesterone-dependent decidualization.

[29] Macdonald LJ, Sales KJ, Grant V et al. Prokineticin 1 induces Dickkopf 1 expression and regulates cell proliferation and decidualization in the human endometrium. ***Mol. Hum. Reprod.*** 17(10), 626-636 (2011).

[30] Camden AJ, Szwarc MM, Chadchan SB et al. Growth regulation by estrogen in breast cancer 1 (GREB1) is a novel progesterone-responsive gene required for human endometrial stromal decidualization. ***Mol. Hum. Reprod.*** 23(9), 646-653 (2017).

[31] Kuroda K, Venkatakrishnan R, Salker MS et al. Induction of 11β-HSD 1 and activation of distinct mineralocorticoid receptor- and glucocorticoid receptor-dependent gene networks in decidualizing human endometrial stromal cells. ***Mol. Endocrinol.*** 27(2), 192-202 (2013).

[32] Almada M, Amaral C, Diniz-da-Costa M et al. The endocannabinoid anandamide impairs in vitro decidualization of human cells. ***Reproduction*** 152(4), 351-361 (2016).

[33] Sun X, Deng W, Li Y et al. Sustained Endocannabinoid Signaling Compromises Decidual Function and Promotes Inflammation-induced Preterm Birth. ***J. Biol. Chem.*** 291(15), 8231-8240 (2016).

[34] Bariani MV, Domínguez Rubio AP, Cella M et al. Role of the endocannabinoid system in the mechanisms involved in the LPS-induced preterm labor. ***Reproduction*** 150(6), 463-472 (2015).

[35] Economos K, MacDonald PC, Casey ML. Endothelin-1 gene expression and protein biosynthesis in human endometrium: potential modulator of endometrial blood flow. ***J. Clin Endocrino.l Metab.*** 74(1), 14-19 (1992).

[36] Gibson DA, Simitsidellis I, Cousins FL et al. Intracrine Androgens Enhance Decidualization and Modulate Expression of Human Endometrial Receptivity Genes. ***Sci. Rep.*** 28(6), 19970 (2016).

[37] Elnashar AM, Aboul-Enein GI. Endometrial receptivity. ***Middle East Fertility Society Journal*** 9(1), 10-24 (2004).

[38] Li JY, Paragas N, Ned RM et al. Scara5 is a ferritin receptor mediating non-transferrin iron delivery. ***Dev. Cell.*** 16(1), 35-46 (2009).

[39] Lee J, Oh JS, Cho C. Impaired expansion of trophoblast spheroids cocultured with endometrial cells overexpressing cellular retinoic acid-binding protein 2. ***Fertil. Steril.*** 95(8), 2599-2601 (2011).

[40] Sherafat-Kazemzadeh R, Schroeder JK, Kessler CA et al. Parathyroid hormone-like hormone (PTHLH) represses decidualization of human uterine fibroblast cells by an autocrine/paracrine mechanism. ***J. Clin. Endocrinol. Metab.*** 96(2), 509-514 (2011).

[41] Ozaki R, Kuroda K, Ikemoto Y, et al. Reprogramming of the retinoic acid pathway in decidualizing human endometrial stromal cells. ***PLoS One*** 2017 12:e0173035 (2017).

[42] Dyson MT, Roqueiro D, Monsivais D et al. Genome-wide DNA methylation analysis predicts an epigenetic switch for GATA factor expression in endometriosis. ***PLoS Genet.*** 10(3), e1004158 (2014).

[43] Lucas ES, Dyer NP, Murakami K et al. Loss of Endometrial Plasticity in Recurrent Pregnancy Loss. ***Stem Cells*** 34(2), 346-356 (2016).

[44] Zondervan KT, Rahmioglu N, Morris AP et al. Beyond Endometriosis Genome-Wide Association Study: From Genomics to Phenomics to the Patient. ***Semin Reprod Med.*** 34(4):242-54 (2016).

[45] Fung JN, Girling JE, Lukowski SW et al. The genetic regulation of transcription in human endometrial tissue. ***Hum Reprod.*** 32(4):893-904 (2017).

563 ***Figure Legends***

564 **Fig.1: Transcriptome profiling of ESCs (D0) and decidualized cells (D4 and D8) from two independent**
565 **donors**

566 **A.** Cell culture scheme for *in vitro* decidualization. Detailed procedures are described in **the Materials and**
567 **Methods**. Blue and red arrows indicate the periods of cell culture with cell maintenance medium and
568 differentiation medium, respectively. Microscopic photographs (x200) of cells are shown. **B.** Series of cells (D0,
569 D4, and D8) from two donors (EM0409 and EM0519) were assessed for the expression levels of *PRL* and *IGFBP1*
570 upon decidualization (D4 and D8) relative to those in control D0 cells by quantitative RT-PCR (one point
571 measurement per sample). **C.** Numbers of differentially expressed genes series upon decidualization. **D.**
572 Representative GO terms enriched in up- and down-regulated genes upon decidualization.

573

574 **Fig.2: Evaluation of correlation of transcriptome and epigenome profiles between two donors and**
575 **between ESCs and decidualized cells**

576 **A.** Comparisons of genome-wide DNA methylation profiles among D0, D4, and D8 cells from the EM0409 donor.
577 **B.** Scatter plots and Pearson correlation coefficients for genome-wide histone modification profiles (H3K27me3,
578 H3K27ac, and H3K9me3) and transcriptome (RNA-seq) profiles. Comparisons were made for all possible
579 pairwise combination among five (H3K27ac) or six samples. Normalized mapped read counts per 1000-bp
580 window for H3K9me3 and H3K27me3, normalized mapped read counts per peak for H3K27ac, and FPKM values
581 for RNA-seq were plotted and assessed for their correlation using the *pairs.panels* function in the psych package
582 of R. The correlation ellipse is shown in red in each plot. Correlation coefficients from the comparison of the same
583 cell type between donors are boxed in blue, those from the comparison of different cell types (D0, D4, or D8)
584 derived from the same donor are boxed in red.

585

586 **Fig.3: Gene expression and histone modification correlations in decidualization**

A. Correlation analyses of GE changes (log2 fold-change (fc) of FPKM values) and HM changes (log 2 fc of enrichment scores) at the gene promoter regions (-2,000 to 0 bp regions relative to TSS) in D4 cells compared to D0 cells for H3K27ac (left), H3K27me3 (middle), and H3K9me3 (right). The numbers of TSSs subjected to the correlation analysis were, 17,462, 11,162, and 6,250 among 23,553 TSSs.

B. Average profiles of three histone modifications along gene structure drawn using the *ngs.plot* software package for four gene groups categorized by GE levels (no, low, middle, and high). **C.** Average profiles of three histone modifications along the structures of up- and down-regulated genes in D0, D4, and D8 cells of EM0409. In panels **B** and **C**, 2000bp upstream, gene body (from TSS to transcription end site (TES)), and 2000bp downstream regions were subjected to count reads. and the averages of the reads per million values of genes were plotted for 101 sub-windows.

Fig.4: Genes up- and down-regulated upon decidualization accompanied with reciprocal changes of H3K27ac and H3K27me3 levels at their promoter region

A. Box plot representation of gene expression fold changes of all 21,753 TSSs, TSSs accompanied with H3K27ac change only (orange and light blue), and TSSs accompanied with reciprocal changes of H3K27ac and H3K27me3 in EM0409 cell series (red and blue). The 21,753 TSSs were selected as those whose FPKM value is greater than 0.3 in one or more of three cell types (D0, D4, and D8). **B.** Scatter plot representation of log2-transformed FPKM values in EM0409_D0 (x-axis) and EM0409_D4 (y-axis) cells. The color assignment for dots and lines is the same as that in panel A. Lines represent the median of log2-transformed FPKM fold-changes of each of sub-categories. **C.** Heatmap representation of the H3K27ac and H3K27me3 enrichment levels of 23 up-regulated and 8 down-regulated promoters accompanied with reciprocal changes of H3K27ac and H3K27me3. These were selected as those fulfilling the FPKM log2 fold-change criteria of > 4 or < -4. #1 and #2 correspond to EM0409 and EM0519. The heatmap color scales are shown at the bottom. **D.** Visualization of histone modification and gene expression alterations for six loci. Read count (per 25bp-window) data (in .tdf format) were created using

611 the *count* function of IGVtools (https://software.broadinstitute.org/software/igv/igvtools) from the mapped results
612 of ChIP-seq and RNA-seq data (.bam files), and visualized using the Integrative Genomics Viewer (IGV,
613 http://software.broadinstitute.org/software/igv/). The asterisk in the panels for *WNT4*, *ZBTB16*, *HSD11B1*, and
614 *ADRA2A* indicates the approximate position of the genomic interval showing reciprocal changes of H3K27ac and
615 H3K27me3 upon decidualization.

List of Supplementary Materials

Table S1: Clinical characteristics of donor individuals

Table S2: Summary of mapping and PCR-duplicate metrics for RNA-seq and ChIP-seq libraries, and ChIP-seq peaks detected by MACS2

Table S3: List of differentially expressed genes upon decidualization of endometrial stromal cells (ESCs)

Table S4: Top Gene Ontology terms enriched among differentially expressed genes upon decidualization of endometrial stromal cells (ESCs)

Table S5: Summary for the numbers of H3K27ac peaks and H3K27me3/H3K9me3 windows showing increased or decreased enrichment scores upon decidualization

Table S6: Summary for the correlation analyses of gene expression and histone modification changes at the gene promoter regions upon decidualization

Table S7: List of transcription start sites (TSSs) accompanied with H3K27ac increase or decrease upon decidualization at their 2,000 bp upstream region (corresponding to the TSSs selected as orange, red, light blue, and blue sub-categories in Fig.4A and 4B)

Table S8: List of promoter regions accompanied with reciprocal changes of H3K27ac and H3K27me3 modifications upon decidualization (including the loci shown in Fig.4C)

Table S9: Evaluation of the extents of gene activation and repression upon decidualization for the gene sets with reciprocal changes of H3K27ac and H3K27me3 at their promoter region and for the gene sets with H3K27ac change only

Figure S1: Average profiles of three histone modifications along the structures of up- and down-regulated genes in D4 cells compared to D0 cells

Figure S2: Wilcoxon rank sum test p-values for pair-wise comparisons among all TSSs and TSS sub-categories shown in Fig.4A

Figure S3: Transcriptome and histone modification profiles obtained for ESCs (D0) and decidualized cells (D4

and D8) from two donors (EM0409 and EM0519) visualized using the Integrative Genomics Viewer (IGV, http://software.broadinstitute.org/software/igv/). A 231 kb interval including the *WNT4* locus is shown as an example. All bigwig files (.bw) visualized in this figure are available at http://tapir.zednet.jp/data/suppl/bigwig_files.zip. Bam files without PCR duplicate reads were converted to wig files using igvtools (*count* command with options "- z 5 -w 25"), and further converted to bigwig files (.bw) using the wigToBigWig script (http://hgdownload.cse.ucsc.edu/admin/exe/).

List of download URLs (and data size) for supplemental datasets

http://tapir.zednet.jp/data/suppl/TableS3_180418.xlsx (519 KB)

http://tapir.zednet.jp/data/suppl/TableS7_180418.xlsx (624 KB)

http://tapir.zednet.jp/data/suppl/macs2.peakcalls.zip (212 MB)

http://tapir.zednet.jp/data/suppl/fpkm_tracking.zip (32 MB)

http://tapir.zednet.jp/data/suppl/bigwig_files.zip (6.2 GB)

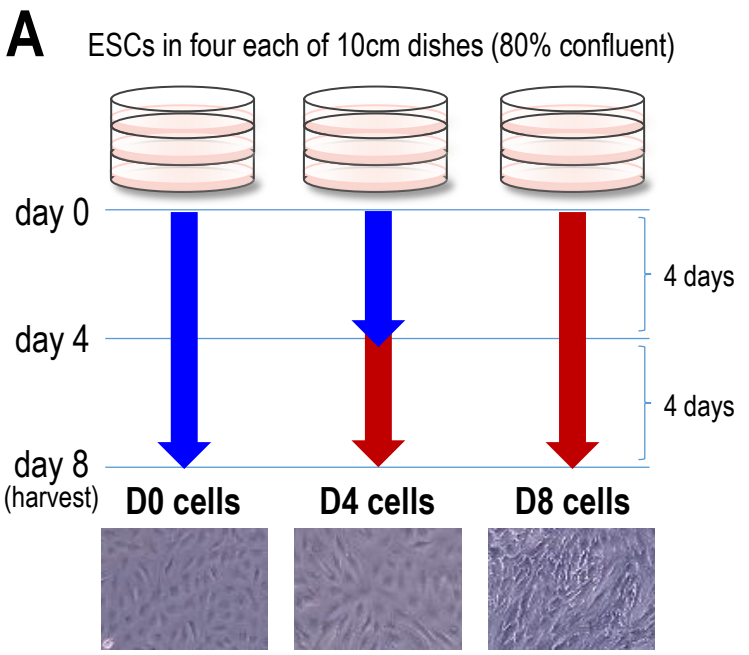

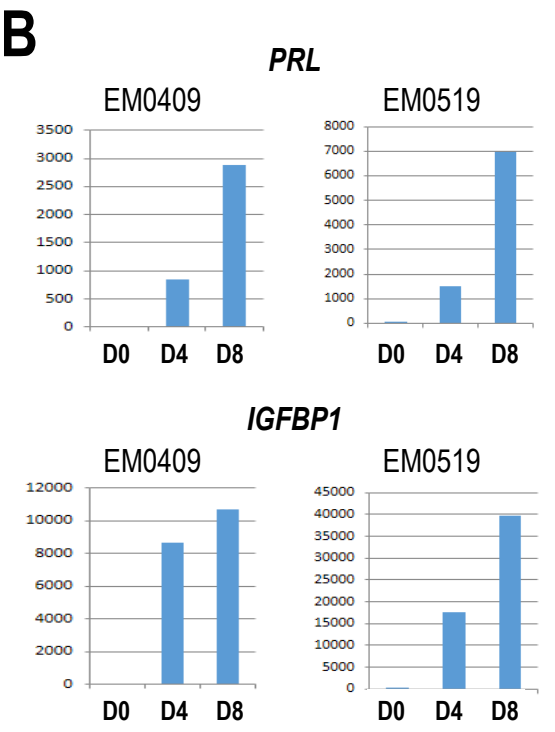

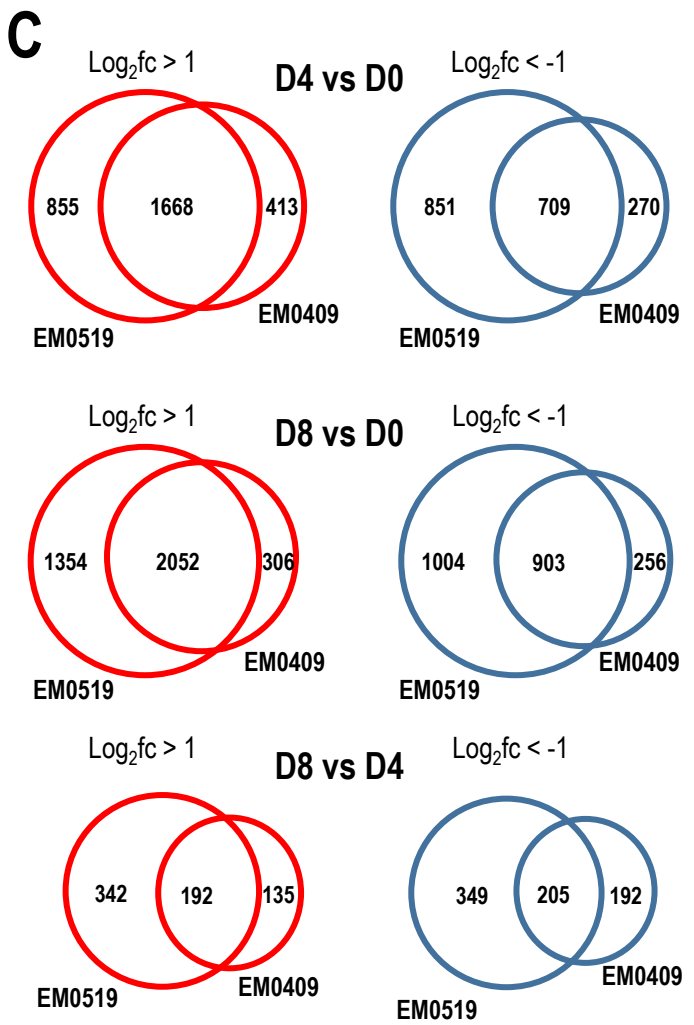

D

GO terms enriched among 2,055 up-regulated genes in D8 cells compared to D0 cells

GO term	Count	*P*-Value
oxidation-reduction process	104	1.9E-08
cholesterol biosynthetic process	18	3.8E-08
lipid metabolic process	38	6.5E-07
carbohydrate metabolic process	39	3.4E-06
extracellular matrix organization	40	2.5E-05

GO terms enriched among 905 down-regulated genes in D8 cells compared to D0 cells

GO Term	Count	*P*-Value
nucleosome assembly	30	2.9E-14
extracellular matrix organization	28	1.5E-07
DNA replication	22	4.7E-06

Fig.1

A

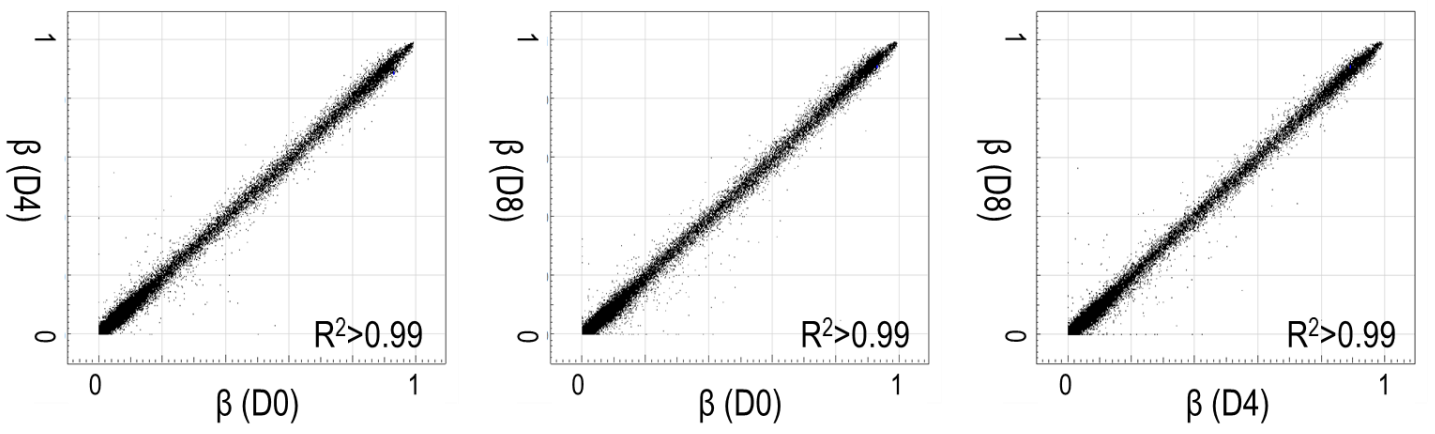
D4 vs D0
D8 vs D0
D8 vs D4
β (D4)
β (D8)
β (D0)
R²>0.99
0
1

B

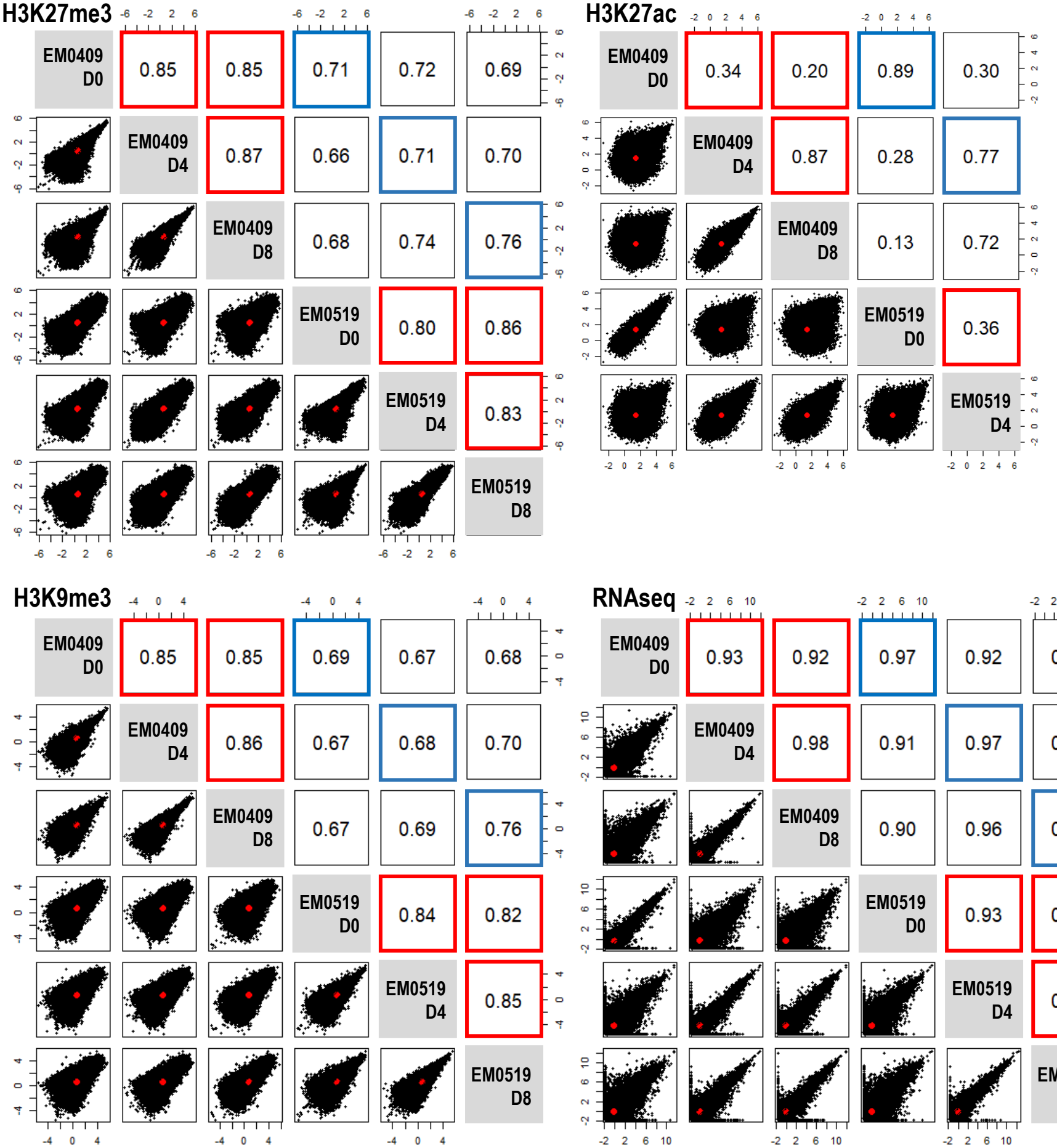
H3K27me3
EM0409 D0
EM0409 D4
EM0409 D8
EM0519 D0
EM0519 D4
EM0519 D8
0.85 0.85 0.71 0.72 0.69
0.87 0.66 0.71 0.70
0.68 0.74 0.76
0.80 0.86
0.83
H3K27ac
0.34 0.20 0.89 0.30
0.87 0.28 0.77
0.13 0.72
0.36
H3K9me3
0.85 0.85 0.69 0.67 0.68
0.86 0.67 0.68 0.70
0.67 0.69 0.76
0.84 0.82
0.85
RNAseq
0.93 0.92 0.97 0.92 0.90
0.98 0.91 0.97 0.96
0.90 0.96 0.97
0.93 0.90
0.98

Fig.2

A

EM0409_D4 vs EM0409_D0

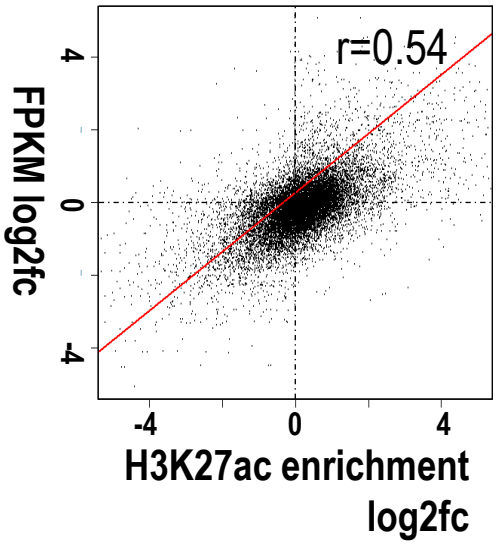

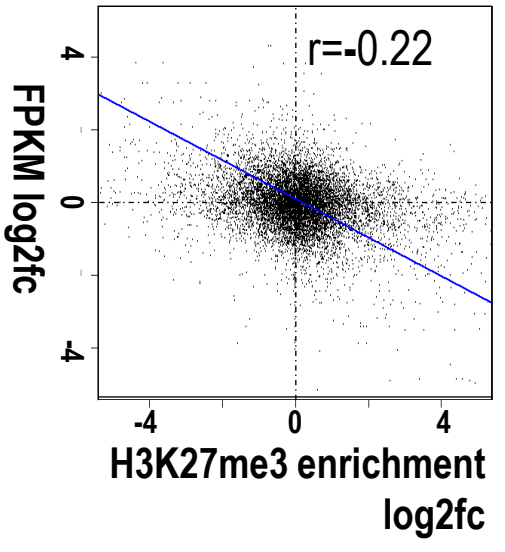

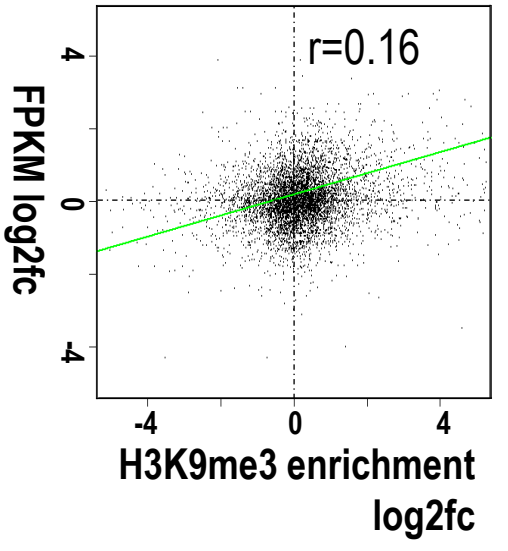

B

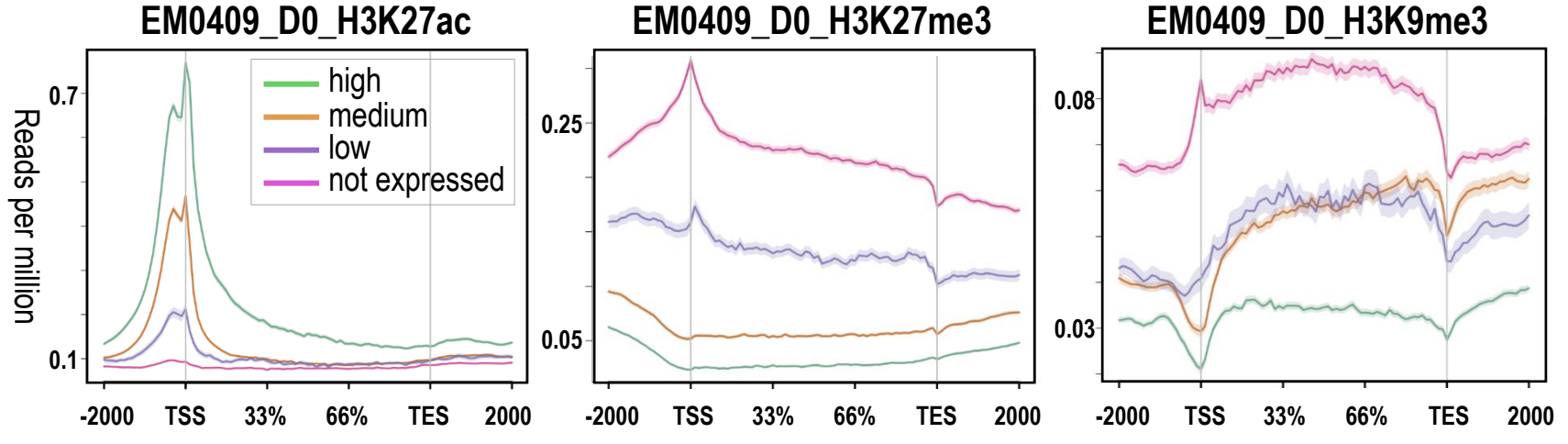

C

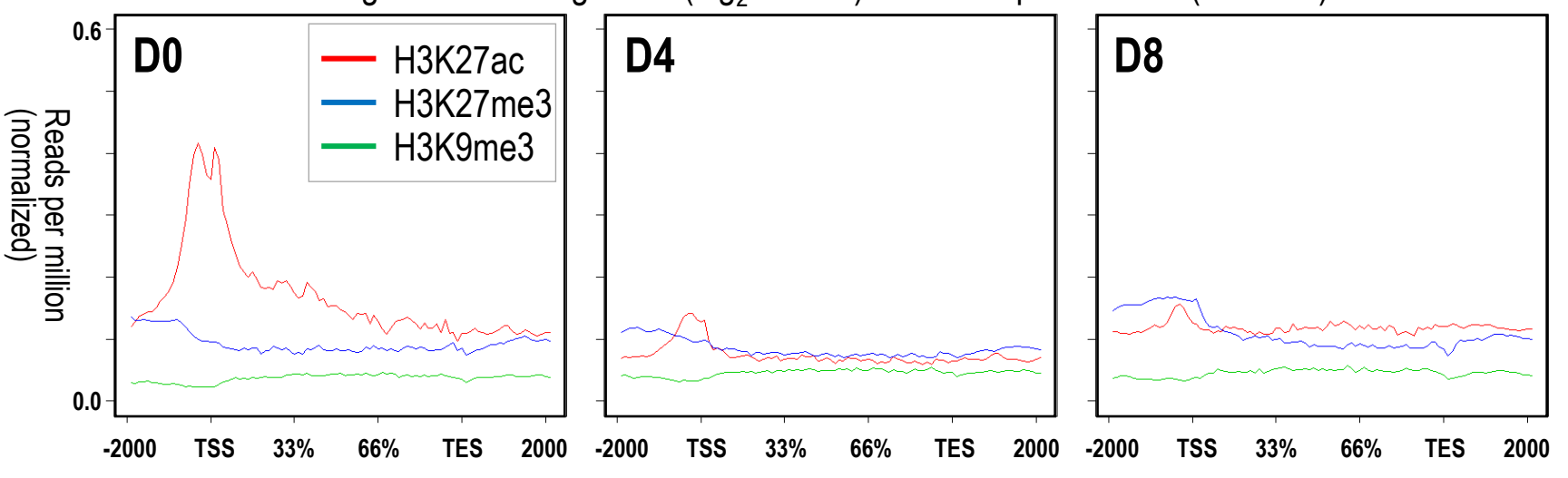

Fig.3

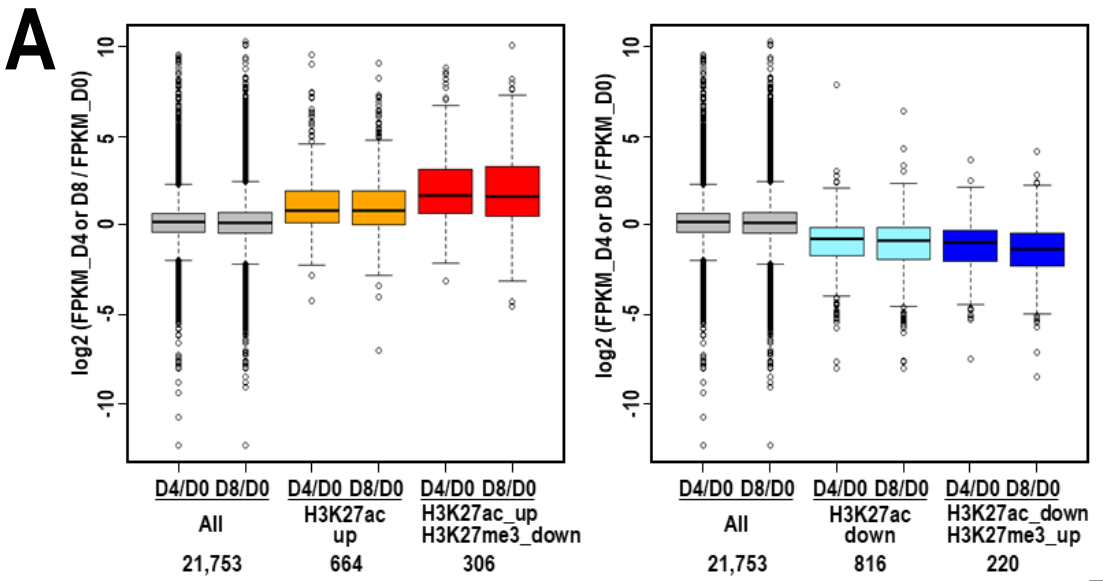

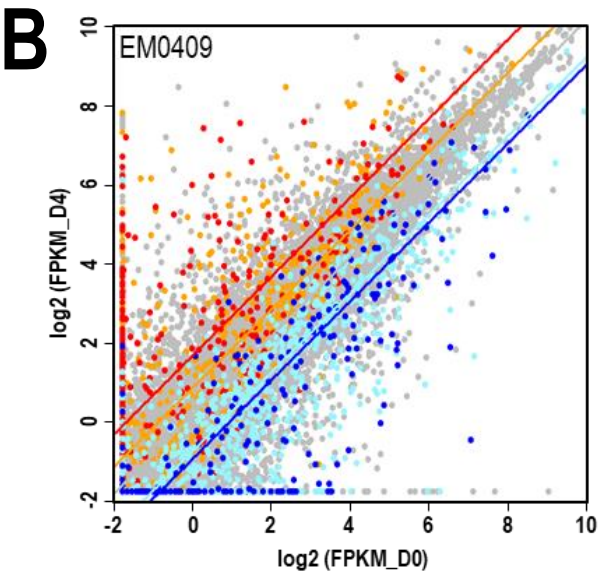

C

	H3K27ac D0 #1	H3K27ac D0 #2	H3K27ac D4 #1	H3K27ac D4 #2	H3K27ac D8 #1	H3K27me3 D0 #1	H3K27me3 D0 #2	H3K27me3 D4 #1	H3K27me3 D4 #2	H3K27me3 D8 #1	H3K27me3 D8 #2	GE D0 #1	GE D0 #2	GE D4 #1	GE D4 #2	GE D8 #1	GE D8 #2	log_2fc D4/D0	log_2fc D8/D0
PCDH20																		9.48	9.44
HSD11B1																		9.28	10.03
LRRC15																		8.71	9.92
CNR1																		8.33	8.30
SCARA5																		8.13	8.55
EDNRB																		7.96	8.21
WNT4																		6.74	7.23
GADD45G																		6.18	6.13
PROK1																		5.64	6.70
GREB1																		5.51	6.03
ATP8A2																		5.47	6.52
ZBTB16																		5.35	5.42
C6orf176																		5.19	4.71
CILP																		5.18	4.83
P4HA3																		5.16	4.65
LOC441177																		4.94	4.48
LGR4																		4.90	5.76
SLC46A2																		4.73	4.33
NTRK1																		4.71	5.46
PRRG4																		4.35	4.61
SERPINB2																		4.31	5.02
SPHK1																		4.29	3.07
LAMC3																		4.10	4.82

	H3K27ac D0 #1	H3K27ac D0 #2	H3K27ac D4 #1	H3K27ac D4 #2	H3K27ac D8 #1	H3K27me3 D0 #1	H3K27me3 D0 #2	H3K27me3 D4 #1	H3K27me3 D4 #2	H3K27me3 D8 #1	H3K27me3 D8 #2	GE D0 #1	GE D0 #2	GE D4 #1	GE D4 #2	GE D8 #1	GE D8 #2	log_2fc D4/D0	log_2fc D8/D0
ADRA2A																		-7.06	-8.17
CRABP2																		-5.38	-5.85
PRELP																		-5.12	-5.78
WNT2																		-4.85	-7.68
TYMS																		-4.85	-4.78
COL16A1																		-4.72	-4.83
PTHLH																		-4.37	-4.37
MRGPRF																		-4.26	-4.93

H3K27ac -3 1 5 (log2)
H3K27me3 -4 1 3 (log2)
GE -2 3 8 (log2)

D

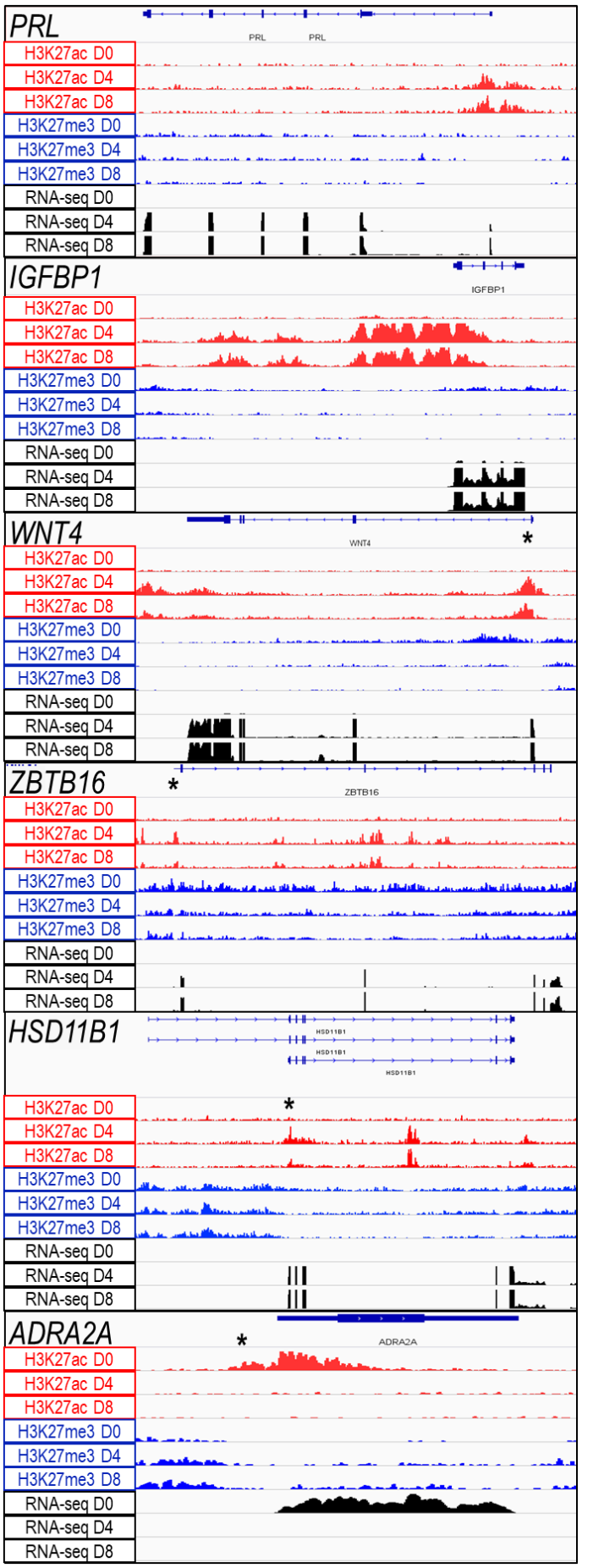

Fig.4

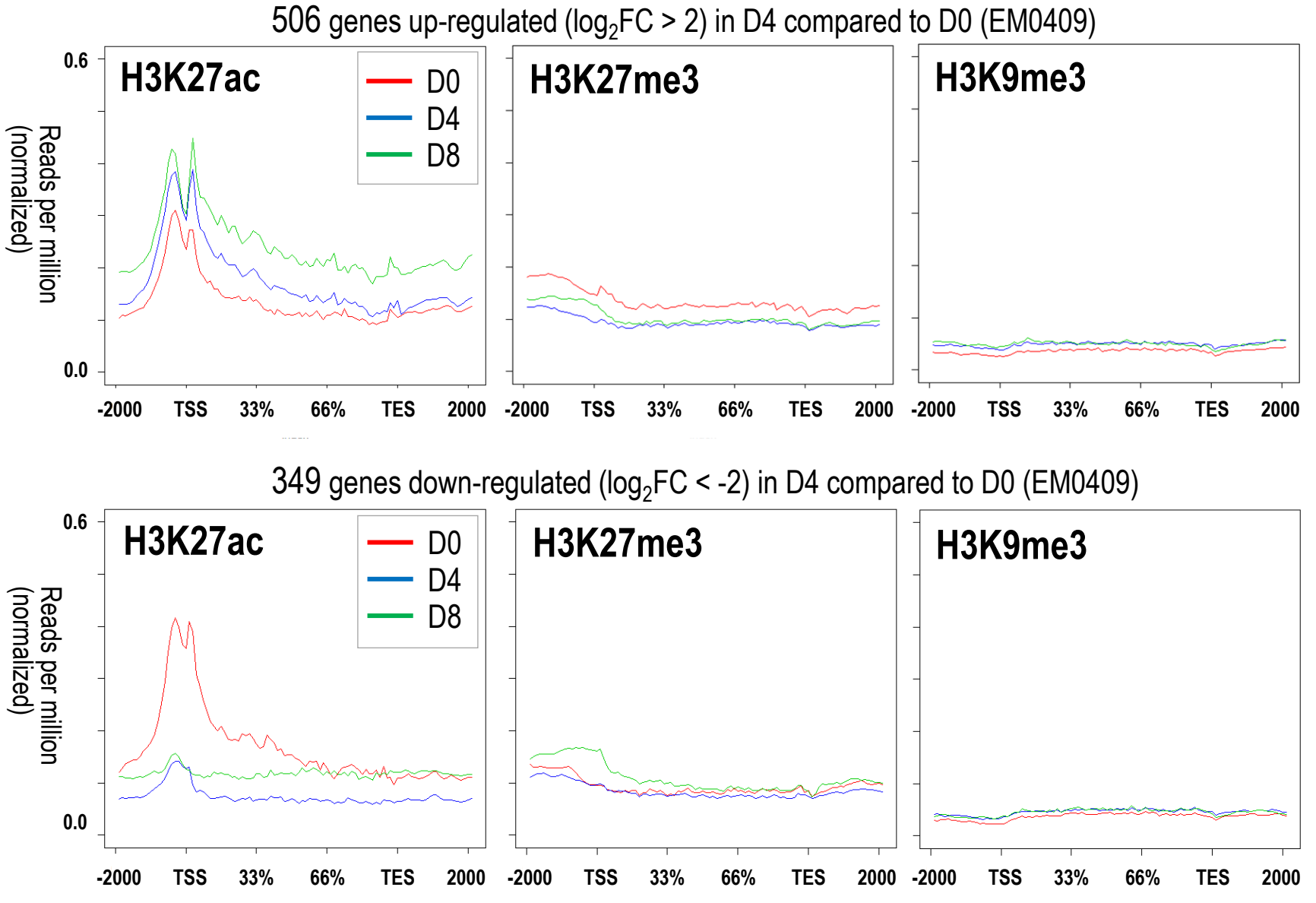

Figure S1: Average profiles of three histone modifications along the structures of 506 up- and 349 down-regulated genes in D4 cells compared to D0 cells.

The 2,000 bp upstream, the gene body (from transcription start site (TSS) to transcription end site (TES)), and the 2,000bp downstream regions were subjected to counting reads. The averages of the normalized reads per million values of the genes were plotted for 101 sub-windows.

Fig.S1

	FPKM fold changes **(D4 vs D0)** of 664 TSSs (H3K27ac ≥ 2 H3K27me3 ≥ 0.5)	FPKM fold changes **(D8 vs D0)** of 664 TSSs (H3K27ac ≥ 2 H3K27me3 ≥ 0.5)	FPKM fold changes **(D4 vs D0)** of 306 TSSs (H3K27ac ≥ 2 H3K27me3 < 0.5)	FPKM fold changes **(D8 vs D0)** of 306 TSSs (H3K27ac ≥ 2 H3K27me3 < 0.5)
FPKM fold changes (D4 vs D0) of all 21,753 TSSs	2.2E-16		2.2E-16	
FPKM fold changes (D8 vs D0) of all 21,753 TSSs		2.2E-16		2.2E-16
FPKM fold changes **(D4 vs D0)** of 664 TSSs (H3K27ac ≥ 2 H3K27me3 ≥ 0.5)			1.6E-12	
FPKM fold changes **(D8 vs D0)** of 664 TSSs (H3K27ac ≥ 2 H3K27me3 ≥ 0.5)				3.9E-10

	FPKM fold changes **(D4 vs D0)** of 816 TSSs (H3K27ac < 0.5 H3K27me3 < 2)	FPKM fold changes **(D8 vs D0)** of 816 TSSs (H3K27ac < 0.5 H3K27me3 < 2)	FPKM fold changes **(D4 vs D0)** of 220 TSSs (H3K27ac < 0.5 H3K27me3 ≥ 2)	FPKM fold changes **(D4 vs D0)** of 220 TSSs (H3K27ac < 0.5 H3K27me3 ≥ 2)
FPKM fold changes (D4 vs D0) of all 21,753 TSSs	2.2E-16		2.2E-16	
FPKM fold changes (D8 vs D0) of all 21,753 TSSs		2.2E-16		2.2E-16
FPKM fold changes **(D4 vs D0)** of 816 TSSs (H3K27ac < 0.5 H3K27me3 < 2)			0.02	
FPKM fold changes **(D8 vs D0)** of 816 TSSs (H3K27ac < 0.5 H3K27me3 < 2)				1.9E-03

Fig. S2: Wilcoxon rank sum test *p* -values for pair-wise comparisons among all TSSs and TSS sub-categories shown in Fig. 4A

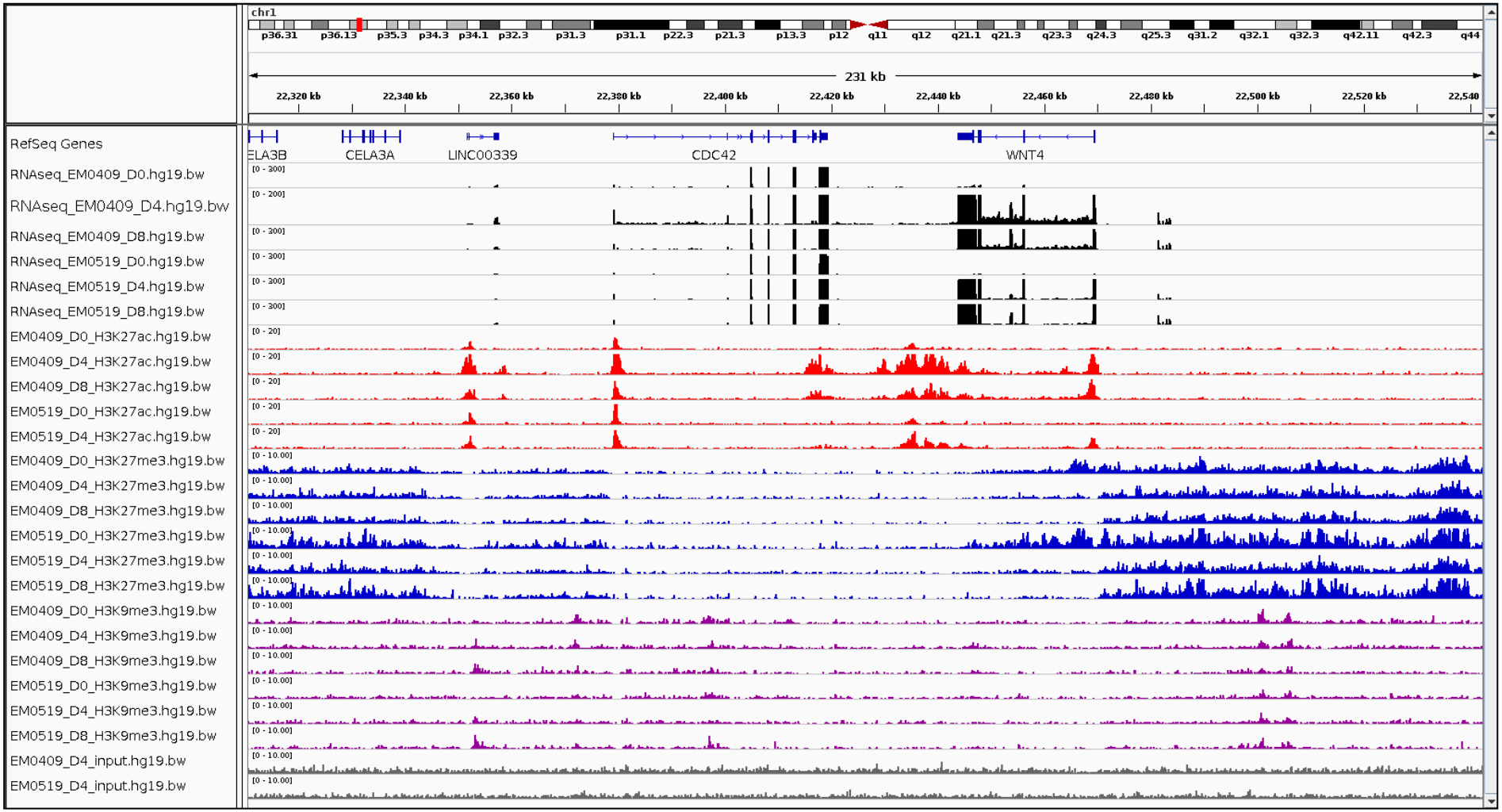

Fig.S3:

Transcriptome and histone modification profiles obtained for ESCs (D0) and decidualized cells (D4 and D8) from two donors (EM0409 and EM0519) visualized using the Integrative Genomics Viewer (IGV, http://software.broadinstitute.org/software/igv/).

A 231 kb interval including the *WNT4* locus is shown as an example. All bigwig files (.bw) visualized in this figure are available at http://tapir.zednet.jp/data/suppl/bigwig_files.zip. Bam files without PCR duplicate reads were converted to wig files using igvtools (*count* command with options "- z 5 -w 25"), and further converted to bigwig files (.bw) using the wigToBigWig script (http://hgdownload.cse.ucsc.edu/admin/exe/).

Table S1: Clinical characteristics of donor individuals

Donor ID	gravidity/ parturition	Age	smoking status	Phases of menstrual cycle at the sampling	Pre-medication	Induction for surgery
EM0409	none	late twenties	none	sceretory phase	none	para-ovarian cyst
EM0519	none	late thirties	none	sceretory phase	none	para-ovarian cyst

Table S2A: Mapping and PCR-duplicate metrics and peak numbers detected by MACS2 for ChP-seq data obtained in this study

ChIP-seq_library_name (Donor_Day_type)	Number of reads examined	Number of unmapped reads	Mapping rate(%)	PCR-duplicate rate (%)	Number of mapped reads (after removing PCR- duplicate reads)	Number of ChIPseq peaks detected by MACS2*
EM0409_D0_H3K27ac	30,835,793	147,210	99.52%	10.94%	27,462,048	40,543
EM0409_D4_H3K27ac	44,773,316	753,360	98.32%	14.78%	38,155,416	46,895
EM0409_D8_H3K27ac	38,183,588	200,829	99.47%	14.09%	32,803,635	26,982
EM0409_D0_H3K27me3	50,039,465	1,768,020	96.47%	14.43%	42,819,470	145,594
EM0409_D4_H3K27me3	57,553,331	2,941,739	94.89%	11.64%	50,852,799	150,192
EM0409_D8_H3K27me3	53,547,182	3,276,283	93.88%	11.85%	47,204,197	136,212
EM0409_D0_H3K9me3	77,700,589	1,219,149	98.43%	25.87%	57,600,223	324,852
EM0409_D4_H3K9me3	64,919,338	890,348	98.63%	22.29%	50,447,324	263,254
EM0409_D8_H3K9me3	54,066,878	1,003,544	98.14%	21.06%	42,682,069	154,263
EM0409_D4_input	78,012,520	491,388	99.37%	7.18%	72,412,859	
EM0519_D0_H3K27ac	44,723,874	295,859	99.34%	12.39%	39,181,513	40,974
EM0519_D4_H3K27ac	32,704,573	199,566	99.39%	8.79%	29,830,397	30,922
EM0519_D8_H3K27ac	92,511,289	635,798	99.31%	7.66%	85,423,259	2
EM0519_D0_H3K27me3	65,645,770	21,762,447	66.85%	12.32%	57,555,914	224,627
EM0519_D4_H3K27me3	57,264,223	10,146,634	82.28%	8.33%	52,492,224	154,420
EM0519_D8_H3K27me3	67,824,112	31,117,014	54.12%	12.89%	59,079,888	214,130
EM0519_D0_H3K9me3	50,471,331	657,894	98.70%	17.06%	41,862,537	201,859
EM0519_D4_H3K9me3	55,096,286	737,055	98.66%	16.51%	45,998,567	241,058
EM0519_D8_H3K9me3	59,006,319	919,242	98.44%	21.46%	46,341,616	295,703
EM0519_D4_input	61,386,390	358,930	99.42%	8.58%	56,116,675	

* Regular peak calling for H3K27ac and input pairs with q-value threshold 0.01, and broad peak calling for H3K27me3 and H3K9me3 using input.bam as a control with broad-cutoff 0.1.

Table S2B: Mapping and PCR-duplicate metrics and peak numbers detected by MACS2 for ChP-seq data presented by Tamura *et al* [21]

ChIP-seq_library_name (treatment, type)	Number of reads examined	Number of unmapped reads	Mapping rate(%)	PCR-duplicate rate (%)	Number of mapped reads (after removing PCR- duplicate reads)	Number of ChIPseq peaks detected by MACS2*
SRR1259174 (EP, H3K27ac)	37,325,445	167678	99.55%	61.10%	14,518,650	9071
SRR1259177 (EP, H3K27me3)	43,001,490	165216	99.62%	46.54%	22,987,307	0
SRR1259178 (EP, input)	39,023,649	154685	99.60%	35.47%	25,180,616	
SRR1259179 (control, H3K27ac)	41,185,692	500044	98.79%	65.54%	14,191,642	2677
SRR1259182 (control, H3K27me3)	31,180,070	362441	98.84%	36.16%	19,905,884	0
SRR1259183 (control, input)	34,711,824	399463	98.85%	39.45%	21,019,098	
SRR1259184 (EP, H3K27ac)	33,032,526	96906	99.71%	46.65%	17,623,015	18764
SRR1259187 (EP, H3K27me3)	41,956,586	113655	99.73%	49.14%	21,339,350	0
SRR1259188 (EP, input)	41,324,972	118578	99.71%	25.30%	30,869,942	
SRR1259189 (control, H3K27ac)	41,347,045	142454	99.66%	40.54%	24,583,774	497
SRR1259192 (control, H3K27me3)	28,636,510	89054	99.69%	31.99%	19,474,289	0
SRR1259193 (control, input)	26,850,846	87234	99.68%	31.49%	18,396,175	

* Regular peak calling for H3K27ac and input pairs with q-value threshold 0.01, and broad peak calling for H3K27me3 using input.bam as a control with broad-cutoff 0.1.

Table S2C: Summary of mapping and PCR-duplicate metrics for RNA-seq libraries

Library_name (Donor_Day_type)	Number of read pairs examined	Mapping rate(%)	PCR-duplicate rate (%)	Number of genes whose FPKM value > 1
RNAseq_EM0409_D0	85,383,973	86.00%	31.35%	44,755
RNAseq_EM0409_D4	86,995,516	86.10%	36.36%	35,039
RNAseq_EM0409_D8	88,221,929	86.00%	39.56%	34,698
RNAseq_EM0519_D0	60,579,013	92.50%	33.19%	42,940
RNAseq_EM0519_D4	62,967,075	92.50%	39.32%	29,818
RNAseq_EM0519_D8	63,179,934	92.40%	41.37%	28,245

Table S4A: Gene Ontology terms (GOTERM_BP_DIRECT) enriched among up-regulated genes upon decidualization of endometrial stromal cells

Gene list	Term (GOTERM_BP_DIRECT)	Count	PValue	Benjamini	Fold Enrich	Genes	List Total	Pop Hits	Pop Total
Up-regulated (FPKM log2 fold-change > 1) in D4 compared to D0 in both EM0409 and EM0519 (1395 gene symbols)	GO:0006695~cholesterol biosynthetic process	22	1.3E-13	5.6E-10	6.97	CYB5R3, TM7SF2, EBP, CES1, MVD, CYP51A1, HMGCR, HMGCS1, FDPS, LSS, FDFT1, APOA1, G6PD, INSIG2, DHCR7, INSIG1, MVK, IDI2, IDI1, HSD17B7, NSDHL, DHCR24	1395	38	16792
	GO:0006629~lipid metabolic process	39	1.2E-09	2.7E-06	2.99	PPARD, LDLR, TRPV1, NAAA, TPRA1, PTGS1, ABHD5, CLU, ABHD4, HMGCS1, APOC1, BTN2A1, GPCPD1, ACAT2, ASAH1, PLCL1, SLC16A1, APOD, PLIN1, PEMT, SRD5A3, HMGCL, SREBF1, FADS1, PTPRN2, CPNE7	1395	157	16792
	GO:0007568~aging	37	6.0E-08	8.9E-05	2.70	TSPO, HMGCR, GRB2, TPRA1, SNCA, NFKB2, IL15, DCN, ADA, TIMP1, EDNRB, ARG1, TNFRSF1B, APOD, CNR1, P2RY1, RPN2, SREBF1, GNAO1, CRYAB, FADS1, PDE4D, SERPING1, PPARGC1A, STAT3, SCAP, CDKN1C	1395	165	16792
	GO:0055114~oxidation-reduction process	87	2.0E-07	2.2E-04	1.77	CYB5R3, TM7SF2, MRPS36, CYB5R1, HTATIP2, ENOX2, ALDH1L1, VKORC1L1, HMGCR, SNCA, PGD, PTGS1, PRDX4, OSGIN2, PDIA5, DHRSX, FDFT1, AKR1C2, PLOD2, PLOD3, P4HA3, CBFG1, GPX3, SRD5A3, SMOX	1395	592	16792
	GO:0030198~extracellular matrix organization	40	2.3E-07	2.0E-04	2.46	SPOCK2, LUM, ADAMTSL4, HSD17B12, ELN, PRDX4, NFKB2, DCN, VIT, ABI3BP, LAMB3, TNFRSF11B, COL7A1, CRISPLD2, ITGB8, COMP, COL27A1, SERPINE1, VWA1, SPP1, COL4A4, COL18A1, COL4A3	1395	196	16792
	GO:0005975~carbohydrate metabolic process	35	2.1E-06	1.5E-03	2.42	MET, TALDO1, GLB1L, ADPGK, GBG11, UGDH, SHPK, GLB1, GPD1L, SLC2A8, UEVLD, ST3GAL5, SLC2A3, NAGA, GK5, INSR, B4GALT4, NANP, B4GALT5, GBA, B4GALNT1, B4GALT3, SLC39A2, CHST2, CHI3L2, BPGM	1395	174	16792
	GO:0042493~response to drug	51	2.3E-06	1.4E-03	2.02	TSPO, ADCY1, STAR, GNA12, SNCA, PNP, TNFRSF11B, APOA1, APOD, RPN2, RET, LYN, RPH3AL, CST3, GAL, PPARGC1A, JUNB, CD38, NPC1, ABAT, HMGCS1, TIMP4, ABCA1, ABCA3, ADA, ARG1, ACSL1, PEMT, COL18A1	1395	304	16792
	GO:0032526~response to retinoic acid	15	2.9E-06	1.6E-03	4.40	SREBF1, RBP4, MICB, SCAMP3, OXT, ACER2, SLC10A3, CD38, DKK1, DUSP1, WNT9B, PTCH1, TIE1, IGFBP2, CTSH	1395	41	16792
	GO:0008299~isoprenoid biosynthetic process	9	4.2E-06	2.1E-03	7.74	MVD, ISPD, HMGCR, FDPS, HMGCS1, MVK, IDI2, IDI1, FDFT1	1395	14	16792
	GO:0008203~cholesterol metabolic process	19	7.2E-06	3.2E-03	3.36	SOAT1, SREBF1, CEBPA, SOAT2, EBP, PPARD, STAR, CYP11A1, LDLR, APOC1, ABCA1, SCAP, SREBF2, CYP7B1, NPC1, APOA1, INSIG2, INSIG1, CLN8	1395	68	16792
	GO:0045444~fat cell differentiation	19	2.1E-05	8.4E-03	3.13	TMEM120A, PID1, SREBF1, CEBPA, METTL8, RNASEL, CEBPD, SMAD6, NR4A1, FOXO1, TTC8, NR4A3, IL11, GPX1, BBS2, GDF10, METRNL, SDF4, KLF4	1395	73	16792
Gene list	Term (GOTERM_BP_DIRECT)	Count	PValue	Benjamini	Fold Enrich	Genes	List Total	Pop Hits	Pop Total
Up-regulated (FPKM log2 fold-change > 1) in D8 compared to D0 in both EM0409 and EM0519 (1693 gene symbols)	GO:0055114~oxidation-reduction process	104	1.9E-08	9.1E-05	1.74	OXA1L, ALDH1L1, VKORC1L1, PTGS1, PGD, SNCA, PLOD2, SMOX, HIGD1A, ALDH6A1, PCBD2, PCBD1, TECR, SCCPDH, PYCR2, ALOX15B, HSD11B1, FDX1L, SURF1, SRXN1, ME1, HSD17B11, HSD17B10, ADHFE1	1693	592	16792
	GO:0006695~cholesterol biosynthetic process	18	3.8E-08	9.1E-05	4.70	CYB5R3, TM7SF2, CES1, MVD, CYP51A1, FDPS, LSS, PMVK, APOA1, G6PD, DHCR7, INSIG1, MVK, IDI2, IDI1, HSD17B7, NSDHL, DHCR24	1693	38	16792
	GO:0006629~lipid metabolic process	38	6.5E-07	1.0E-03	2.40	HSD17B10, PPARD, LDLR, TRPV1, NAAA, PAFAH2, TPRA1, ABHD5, CLU, PTGS1, APOC1, BTN2A1, ACAT2, ASAH1, PLCL1, SLC16A1, APOD, PLIN1, PEMT, SRD5A3, HMGCL, SREBF1, LPL, PLA2G15, FADS1, PTPRN2	1693	157	16792
	GO:0042493~response to drug	58	2.8E-06	3.3E-03	1.89	ALAD, TSPO, ADCY1, STAR, PGF, SNCA, GNA12, SRP19, PNP, SLC1A2, TNFRSF11B, APOA1, APOD, GATA6, GATA3, RPN2, RET, FECH, LYN, CST3, RPH3AL, FOSB, GAL, CD38, NPC1, ABAT, TIMP4, ABCA1, CALB, ABCA3	1693	304	16792
	GO:0005975~carbohydrate metabolic process	39	3.4E-06	3.2E-03	2.22	MET, TALDO1, GLB1L, ADPGK, GBG11, FUCA1, FUCA2, HEXA, HEXB, SHPK, GLB1, GPD1L, SLC2A8, UEVLD, ST3GAL5, SLC2A3, NAGA, GK5, INSR, B4GALT4, B4GALT5, GBA, MGAT4B, B4GALT3, NPL, SLC3A2, CHST2, CHI3L2	1693	174	16792
	GO:0030198~extracellular matrix organization	40	2.5E-05	2.0E-02	2.02	MPZL3, SPOCK2, LUM, WNT3A, ADAMTSL4, HSD17B12, PRDX4, VTN, NFKB2, DCN, ABI3BP, SMOC2, LAMB3, TNFRSF11B, COL7A1, CRISPLD2, ITGB8, COMP, SERPINE1, FBN2, VWA1, FGF2, SPP1, COL4A4, COL4A3	1693	196	16792
Gene list	Term (GOTERM_BP_DIRECT)	Count	PValue	Benjamini	Fold Enrich	Genes	List Total	Pop Hits	Pop Total
Up-regulated (FPKM log2 fold-change > 1) in D8 compared to D4 in both EM0409 and EM0519	No term detected								

Table S4B: Gene Ontology terms (GOTERM_BP_DIRECT) enriched among down-regulated genes upon decidualization of endometrial stromal cells

Gene list	Term (GOTERM_BP_DIRECT)	Count	PValue	Benjamini	Fold Enrich	Genes	List Total	Pop Hits	Pop Total
Down-regulated (FPKM log2 fold-change < -1) in D4 compared to D0 in both EM0409 and EM0519 (574 gene symbols)	GO:0006334~nucleosome assembly	25	1.6E-12	4.2E-09	6.15	HIST1H4I, HIST1H4L, HIST1H2BO, HIST1H2BN, HIST1H4B, HIST1H2BL, HIST1H2BI, HIST3H2BB, HIST1H4I, HIST1H2BD, HIST1H2BE, HIST1H1B, HIST1H2BF, HIST1H1A, HIST1H2BH, MCM2, HIST2H3D	574	119	16792
	GO:0006335~DNA replication-dependent nucleosome assembly	13	2.7E-10	3.5E-07	11.88	HIST4H4, HIST1H4L, HIST1H4B, HIST1H3A, HIST1H3B, HIST1H3C, HIST1H3E, HIST1H3F, HIST1H4I, CHAF1A, HIST1H3G, CHAF1B, HIST1H3H	574	32	16792
	GO:0051290~protein heterotetramerization	13	9.6E-09	8.4E-06	9.05	HIST4H4, HIST1H4L, NLGN1, S100A10, HIST1H4B, HIST1H3A, HIST1H3B, HIST1H3C, HIST1H3E, HIST1H3F, HIST1H4I, HIST1H3G, HIST1H3H	574	42	16792
	GO:0032200~telomere organization	11	9.9E-09	6.5E-06	11.92	HIST1H4L, HIST4H4, HIST1H4B, HIST1H3A, HIST1H3B, HIST1H3C, HIST1H3E, HIST1H3F, HIST1H4I, HIST1H3G, HIST1H3H	574	27	16792
	GO:0000183~chromatin silencing at rDNA	12	2.5E-08	1.3E-05	9.49	HIST1H4L, HIST4H4, HIST1H4B, HIST1H3A, HIST1H3B, HIST1H3C, HIST1H3E, HIST1H3F, HIST1H4I, HIST1H3G, HIST1H3H, HIST2H3D	574	37	16792
	GO:0045814~negative regulation of gene expression, epigenetic	13	8.2E-08	3.6E-05	7.61	HIST4H4, HIST1H4L, EZH2, HIST2H3D, HIST1H4B, HIST1H3A, HIST1H3B, HIST1H3C, HIST1H3E, HIST1H3F, HIST1H4I, HIST1H3G, HIST1H3H	574	50	16792
	GO:0006260~DNA replication	21	3.3E-07	1.2E-04	3.96	RECQL4, CLSPN, CDC6, LIG1, NFIX, RMI2, MCM2, MCM4, MCM5, BRCA1, CDC45, RFC3, MCM7, TIMELESS, PCNA, CHTF18, NFIC, CHAF1A, CHAF1B, NFIA, DSCC1	574	155	16792
	GO:0060968~regulation of gene silencing	7	6.1E-07	2.0E-04	18.62	HIST1H3A, HIST1H3B, HIST1H3C, HIST1H3E, HIST1H3F, HIST1H3G, HIST1H3H	574	11	16792
	GO:0045815~positive regulation of gene expression, epigenetic	12	6.9E-06	2.0E-03	5.66	HIST1H4L, HIST4H4, HIST1H4B, HIST1H3A, HIST1H3B, HIST1H3C, HIST1H3E, HIST1H3F, HIST1H4I, HIST1H3G, HIST1H3H, HIST2H3D	574	62	16792
Gene list	Term (GOTERM_BP_DIRECT)	Count	PValue	Benjamini	Fold Enrich	Genes	List Total	Pop Hits	Pop Total
Down-regulated (FPKM log2 fold-change < -1) in D8 compared to D0 in both EM0409 and EM0519 (743 gene symbols)	GO:0006334~nucleosome assembly	30	2.9E-14	8.9E-11	5.70	HIST1H4L, HIST4H4, HIST1H2BO, HIST1H2BM, HIST1H2BN, HIST1H2BL, HIST1H4B, HIST1H2BI, HIST1H4E, HIST1H4F, HIST1H4C, HIST1H4D, HIST3H2BB, HIST1H4I, HIST1H1D, HIST1H2BD	743	119	16792
	GO:0006335~DNA replication-dependent nucleosome assembly	15	2.2E-11	3.3E-08	10.59	HIST1H4L, HIST4H4, HIST1H4B, HIST1H4E, HIST1H3B, HIST1H4F, HIST1H3C, HIST1H4C, HIST1H4D, HIST1H3F, HIST1H4I, CHAF1A, CHAF1B, HIST1H3G, HIST1H3H	743	32	16792
	GO:0032200~telomere organization	13	4.8E-10	4.8E-07	10.88	HIST4H4, HIST1H4L, HIST1H4B, HIST1H3B, HIST1H4E, HIST1H4F, HIST1H3C, HIST1H4C, HIST1H4D, HIST1H4I, HIST1H3F, HIST1H3G, HIST1H3H	743	27	16792
	GO:0007155~cell adhesion	52	1.3E-09	9.8E-07	2.56	NRP2, ATP1B1, NOAK1, POSTN, EDIL3, CXCL12, WISP1, TGFBI, COL12A1, ROBO2, LOXL2, CYR61, ICAM1, PTPRK, ICAM4, EFNB2, SSPN, DDR1, NCAM2, CNTN1, ADAM12, ACHE, CCL2, CYP1B1, ITGA11, ITGB4, IL32	743	459	16792
	GO:0000183~chromatin silencing at rDNA	14	2.9E-09	1.8E-06	8.55	HIST1H4L, HIST4H4, HIST2H3D, HIST1H4B, HIST1H4E, HIST1H3B, HIST1H4F, HIST1H3C, HIST1H4C, HIST1H4D, HIST1H3F, HIST1H4I, HIST1H3G, HIST1H3H	743	37	16792
	GO:0045814~negative regulation of gene expression, epigenetic	15	2.0E-08	1.0E-05	6.78	HIST1H4L, HIST4H4, EZH2, HIST2H3D, HIST1H4B, HIST1H4E, HIST1H3B, HIST1H4F, HIST1H3C, HIST1H4C, HIST1H4D, HIST1H3F, HIST1H4I, HIST1H3G, HIST1H3H	743	50	16792
	GO:0007275~multicellular organism development	52	8.9E-08	3.9E-05	2.26	PDLIM7, LMO2, LTBP4, JAG1, EDIL3, SPRY4, LBH, FGF1, PHC1, BST2, VANGL2, ENC1, TRERF1, HUNK, FMN2, SERPINF1, HOXD4, TSHZ3, HMGB3, TSHZ1, PAQR8, PAQR5, HIC1, HOXA3, HOXA4, WIPF3, SPATA6	743	521	16792
	GO:0030198~extracellular matrix organization	28	1.5E-07	5.8E-05	3.23	PDGFB, PDGFA, ITGB4, ITGA11, POSTN, ITGAV, COL27A1, TGFBI, COL6A2, COL6A1, THBS1, COL8A1, LAMB1, LOXL1, CYR61, ICAM1, ICAM4, CCDC80, OLFML2A, SPINT1, ITGA4, NDNF, DDR1, LAMA4, BGN	743	196	16792
	GO:0051290~protein heterotetramerization	13	1.7E-07	5.6E-05	7.00	HIST4H4, HIST1H4L, HIST1H4B, HIST1H3B, HIST1H4E, HIST1H4F, HIST1H3C, HIST1H4C, HIST1H4D, HIST1H4I, HIST1H3F, HIST1H3G, HIST1H3H	743	42	16792
	GO:0009611~response to wounding	15	4.8E-07	1.5E-04	5.38	F2RL2, ACHE, NRP1, FGF7, CCL2, PDGFB, PDGFA, ITGB4, AURKA, ABHD2, AGER, TGFB2, ZFP36L1, ZFP36L2, ID3	743	63	16792
	GO:0045815~positive regulation of gene expression, epigenetic	14	2.5E-06	6.8E-04	5.10	HIST1H4L, HIST4H4, HIST2H3D, HIST1H4B, HIST1H4E, HIST1H3B, HIST1H4F, HIST1H3C, HIST1H4C, HIST1H4D, HIST1H3F, HIST1H4I, HIST1H3G, HIST1H3H	743	62	16792
	GO:0006260~DNA replication	22	4.7E-06	1.2E-03	3.21	RECQL4, CLSPN, CDC6, ACHE, LIG1, FAM111A, NFIX, RMI2, MCM2, MCM4, CDK2, MCM5, BRCA1, POLD3, RFC3, MCM7, CHTF18, NFIC, CHAF1A, CHAF1B, NFIA, DSCC1	743	155	16792
	GO:0045653~negative regulation of megakaryocyte differentiatio	8	6.6E-06	1.5E-03	10.04	HIST1H4L, HIST4H4, HIST1H4B, HIST1H4E, HIST1H4F, HIST1H4C, HIST1H4D, HIST1H4I	743	18	16792
Gene list	Term (GOTERM_BP_DIRECT)	Count	PValue	Benjamini	Fold Enrich	Genes	List Total	Pop Hits	Pop Total
Down-regulated (FPKM log2 fold-change < -1) in D8 compared to D4 in both EM0409 and EM0519 (170 gene symbols)	GO:0007155~cell adhesion	27	8.4E-13	1.2E-09	5.81	NRP2, ATP1B1, CYP1B1, PCDHB15, POSTN, EDIL3, CXCL12, VCAM1, S1PR1, COL6A2, COL12A1, COL6A1, LAMB1, THBS2, DPT, COL18A1, ICAM1, CNTN5, ICAM5, COL15A1, COL16A1, HES1, NCAM1, CDH13, ITGA5	170	459	16792
	GO:0030198~extracellular matrix organization	18	1.3E-11	9.9E-09	9.07	COL18A1, ICAM1, ICAM5, ELN, OLFML2A, POSTN, COL5A3, COL16A1, NDNF, VCAM1, COL9A2, ITGA5, COL1A2, COL6A2, COL6A1, VCAN, COL1A1, LAMB1	170	196	16792
	GO:0030199~collagen fibril organization	8	1.1E-07	5.3E-05	20.26	CYP1B1, COL1A2, COL12A1, COL1A1, COL5A3, GREM1, TGFB2, DPT	170	39	16792
	GO:0030574~collagen catabolic process	9	2.4E-07	9.0E-05	13.89	COL18A1, MMP10, COL1A2, COL6A2, COL15A1, COL12A1, COL6A1, COL1A1, COL5A3	170	64	16792
	GO:0001525~angiogenesis	12	1.6E-05	4.8E-03	5.32	NRP2, COL18A1, CYP1B1, S1PR1, EREG, ID1, ITGA5, COL15A1, FGF10, ENPEP, NDNF, TGFB2	170	223	16792

Table S5:
Summary for the numbers of H3K27ac peaks and H3K27me3/H3K9me3 windows showing increased or decreased enrichment scores upon decidualization

H3K27ac (64,497 peaks)	fold-change > 2			fold-change < 0.5		
	EM0409	EM0519	common	EM0409	EM0519	common
D4 vs D0	14,807 23.0%	13,894 21.5%	9,951 15.4%	15,196 23.6%	14,378 22.3%	10,788 16.7%
D8 vs D0	15,900 24.7%			16,565 25.7%		
D8 vs D4	3,609 5.6%			2,332 3.6%		

H3K27me3 (1,280,496 windows*)	fold-change > 2			fold-change < 0.5		
	EM0409	EM0519	common	EM0409	EM0519	common
D4 vs D0	42,525 3.3%	43,173 3.4%	3,790 0.3%	63,257 4.9%	66,964 5.2%	9,384 0.7%
D8 vs D0	38,755 3.0%	41,468 3.2%	7,675 0.6%	33,448 2.6%	38,629 3.0%	11,845 0.9%
D8 vs D4	35,211 2.7%	37,979 3.0%	5,668 0.4%	57,539 4.5%	51,974 4.1%	4,131 0.3%

* 1000 bp window

H3K9me3 (920,113 windows*)	fold-change > 2			fold-change < 0.5		
	EM0409	EM0519	common	EM0409	EM0519	common
D4 vs D0	30,137 3.3%	26,807 2.9%	3,199 0.3%	30,193 3.3%	29,370 3.2%	3,005 0.3%
D8 vs D0	30,770 3.3%	27,588 3.0%	8,620 0.9%	35,398 3.8%	33,057 3.6%	5,331 0.6%
D8 vs D4	24,139 2.6%	25,330 2.8%	3,172 0.3%	27,914 3.0%	29,145 3.2%	2,896 0.3%

* 1000 bp window

Table S6: Summary for the correlation analyses of gene expression and histone modification changes at the gene promoter regions upon decidualization

Histone type and distance to TSS	D4 vs D0			
	EM0409		EM0519	
	# of TSSs	correlation r	# of TSSs	correlation r
H3K27ac				
no limit	23,553	0.455	23,694	0.442
within 5,000 bp	18,570	0.531	18,548	0.511
within 3,000 bp	18,003	0.537	17,975	0.518
within 2,000 bp	17,462	0.541	17,624	0.523
H3K27me3				
no limit	23,553	-0.140	23,694	-0.148
within 5,000 bp	15,819	-0.180	15,997	-0.180
within 3,000 bp	13,357	-0.211	13,564	-0.190
within 2,000 bp	11,162	-0.228	11,368	-0.203
H3K9me3				
no limit	23,553	0.090	23,694	0.054
within 5,000 bp	10,623	0.146	10,723	0.084
within 3,000 bp	7,863	0.158	7,938	0.079
within 2,000 bp	6,250	0.161	6,287	0.090

Table S8A: List of up-regulated promoter regions accompanied with reciprocal changes of H3K27ac and H3K27me3 modifications upon decidualization (125 TSSs of 90 RefSeq genes) (1/2)

Locus	Normalized enrichment scores for H3K27ac window (4,000bp)							Normalized enrichment scores for H3K27me3 window (1,000bp)							FPKM values of the TSS located wihtin 5,000bp from the H3K27ac window							
	Chromosome	Start (hg19)	End (hg19)	EM0409D0_K27ac_log2	EM0519D0_K27ac_log2	EM0409D4_K27ac_log2	EM0519D4_K27ac_log2	Chromosome	Start (hg19)	End (hg19)	EM0409D0_K27me3_log2	EM0519D0_K27me3_log2	EM0409D4_K27me3_log2	EM0519D4_K27me3_log2	Chromosome	Start (hg19)	End (hg19)	EM0409D0_fpkm_log2	EM0519D0_fpkm_log2	EM0409D4_fpkm_log2	EM0519D4_fpkm_log2	Distance of TSS to the center of the H3K27ac window (4,000bp)
SAMD11	chr1	858,034	862,034	-0.06	0.44	2.65	2.09	chr1	858,000	859,000	0.80	1.32	-0.58	-1.36	chr1	861,121	861,122	0.73	1.72	4.62	5.12	1,087
TNFRSF1B	chr1	12,225,542	12,229,542	-0.46	-0.16	0.74	1.54	chr1	12,227,000	12,228,000	1.09	0.81	-0.58	-1.27	chr1	12,227,060	12,227,061	1.27	1.77	4.57	5.58	482
CDA	chr1	20,914,241	20,918,241	0.66	-0.58	2.01	0.72	chr1	20,914,000	20,915,000	-0.84	1.07	-2.44	-0.90	chr1	20,915,444	20,915,445	2.16	-0.36	3.59	1.71	797
WNT4	chr1	22,446,500	22,450,500	-1.11	-1.31	0.89	0.78	chr1	22,447,000	22,448,000	-0.29	0.57	-1.84	-1.28	chr1	22,446,747	22,446,748	-1.74	-1.74	1.99	1.56	1,753
WNT4	chr1	22,467,020	22,471,020	-0.01	-0.42	3.71	2.97	chr1	22,469,000	22,470,000	0.78	0.05	-3.78	-2.95	chr1	22,469,518	22,469,519	0.76	-0.06	7.18	7.01	498
WNT4	chr1	22,467,020	22,471,020	-0.01	-0.42	3.71	2.97	chr1	22,469,000	22,470,000	0.78	0.05	-3.78	-2.95	chr1	22,469,986	22,469,987	-1.74	-1.74	3.21	5.42	966
TIE1	chr1	43,766,307	43,770,307	-0.74	-1.21	1.09	1.03	chr1	43,768,000	43,769,000	-0.56	1.10	-3.10	-2.40	chr1	43,766,644	43,766,645	-1.74	-1.74	-0.50	-0.73	1,663
PROK1	chr1	110,991,271	110,995,271	-1.09	-0.49	1.18	1.41	chr1	110,993,000	110,994,000	2.33	2.08	-0.72	-1.61	chr1	110,993,697	110,993,698	-1.74	-1.74	3.48	4.34	426
NTRK1	chr1	156,782,048	156,786,048	-0.59	-0.27	2.26	1.44	chr1	156,784,000	156,785,000	0.50	0.93	-0.70	-1.99	chr1	156,785,344	156,785,345	-1.74	-1.74	2.85	3.10	1,296
NTRK1	chr1	156,782,048	156,786,048	-0.59	-0.27	2.26	1.44	chr1	156,785,000	156,786,000	0.41	0.69	-4.18	-3.84	chr1	156,785,542	156,785,543	-1.74	-1.74	2.70	2.24	1,494
SH2D2A	chr1	156,782,048	156,786,048	-0.59	-0.27	2.26	1.44	chr1	156,785,000	156,786,000	0.41	0.69	-4.18	-3.84	chr1	156,785,938	156,785,939	-1.74	-1.74	1.67	2.60	1,890
SH2D2A	chr1	156,784,136	156,788,136	-0.57	-1.16	2.98	2.84	chr1	156,786,000	156,787,000	0.55	1.89	-4.88	-3.25	chr1	156,786,639	156,786,640	-1.74	-1.74	1.50	1.43	503
CREG1	chr1	167,516,362	167,520,362	-0.88	-0.45	1.48	0.80	chr1	167,519,000	167,520,000	0.02	0.20	-1.16	-1.19	chr1	167,523,061	167,523,062	4.12	4.02	6.59	6.26	4,699
RNASEL	chr1	182,562,402	182,566,402	-1.49	-1.48	1.66	0.93	chr1	182,566,000	182,567,000	0.46	1.22	-1.57	-0.69	chr1	182,558,393	182,558,394	2.67	2.41	3.73	3.75	6,009
RGS16	chr1	182,570,891	182,574,891	-0.74	-1.11	1.58	1.28	chr1	182,572,000	182,573,000	-0.45	0.73	-2.26	-2.60	chr1	182,573,547	182,573,548	0.33	-0.80	3.96	3.52	656
LAMB3	chr1	209,820,499	209,824,499	-0.30	-0.61	0.94	1.32	chr1	209,820,000	209,821,000	1.58	0.19	-0.57	-1.85	chr1	209,824,746	209,824,747	-1.74	-1.74	0.71	1.07	2,247
HSD11B1	chr1	209,878,034	209,882,034	-1.30	-2.44	0.95	0.58	chr1	209,878,000	209,879,000	0.55	0.28	-3.29	-1.69	chr1	209,878,136	209,878,137	-1.74	-1.74	7.73	7.37	1,898
LEFTY2	chr1	226,132,018	226,136,018	-1.36	-0.75	1.12	0.43	chr1	226,132,000	226,133,000	0.87	0.60	-1.27	-0.43	chr1	226,129,082	226,129,083	-1.74	-1.74	4.81	1.67	4,936
LOC100507127	chr10	6,817,949	6,821,949	-0.32	-1.05	2.77	2.13	chr10	6,817,000	6,818,000	-0.38	-0.21	-3.20	-2.91	chr10	6,821,281	6,821,282	-1.74	-1.74	3.53	2.09	1,332
LOC100507127	chr10	6,817,949	6,821,949	-0.32	-1.05	2.77	2.13	chr10	6,817,000	6,818,000	-0.38	-0.21	-3.20	-2.91	chr10	6,821,560	6,821,561	-1.74	-1.74	3.85	1.49	1,611
PSD	chr10	104,165,328	104,169,328	-0.68	-0.82	1.03	0.96	chr10	104,166,000	104,167,000	-0.18	1.07	-2.12	-0.57	chr10	104,164,939	104,164,940	0.98	1.81	2.65	3.72	2,389
PSD	chr10	104,166,632	104,170,632	-0.06	0.09	1.24	1.18	chr10	104,167,000	104,168,000	1.35	2.15	-0.04	0.12	chr10	104,170,080	104,170,081	0.88	0.93	2.26	3.33	1,448
FAM53B	chr10	126,424,924	126,428,924	-1.09	-1.22	1.30	0.36	chr10	126,424,000	126,425,000	0.17	0.61	-2.67	-3.05	chr10	126,432,929	126,432,930	2.33	2.28	5.30	4.64	6,005
GALNTL4	chr11	11,643,043	11,647,043	-1.68	-1.35	1.38	0.66	chr11	11,645,000	11,646,000	0.01	0.50	-2.20	-1.54	chr11	11,643,590	11,643,591	2.39	3.14	4.70	5.27	1,453
ARNTL	chr11	13,296,834	13,300,834	0.38	1.22	2.14	3.06	chr11	13,300,000	13,301,000	1.26	0.09	-0.03	-1.96	chr11	13,299,307	13,299,308	0.60	1.32	3.16	3.62	473
LGR4	chr11	27,497,185	27,501,185	-1.52	-0.95	0.91	0.61	chr11	27,498,000	27,499,000	0.55	0.55	-0.88	-0.95	chr11	27,494,527	27,494,528	0.01	0.36	4.86	5.30	4,658
PRRG4	chr11	32,849,657	32,853,657	-1.32	-0.38	0.91	1.46	chr11	32,853,000	32,854,000	0.41	0.67	-1.45	-1.76	chr11	32,851,154	32,851,155	-1.74	-1.74	-0.15	0.06	503
PRRG4	chr11	32,849,657	32,853,657	-1.32	-0.38	0.91	1.46	chr11	32,853,000	32,854,000	0.41	0.67	-1.45	-1.76	chr11	32,851,316	32,851,317	-1.74	-1.37	1.62	2.52	341
PRRG4	chr11	32,849,657	32,853,657	-1.32	-0.38	0.91	1.46	chr11	32,853,000	32,854,000	0.41	0.67	-1.45	-1.76	chr11	32,851,481	32,851,482	-1.65	-1.74	2.65	2.66	176
RASGRP2	chr11	64,501,288	64,505,288	-0.62	-0.80	3.25	2.09	chr11	64,503,000	64,504,000	0.74	0.77	-1.50	-0.50	chr11	64,504,262	64,504,263	-1.04	-0.74	1.13	1.64	974
RASGRP2	chr11	64,509,093	64,513,093	0.42	1.10	2.80	3.43	chr11	64,509,000	64,510,000	-0.50	0.27	-2.52	-1.73	chr11	64,510,741	64,510,742	-1.02	1.32	2.81	3.97	352
RASGRP2	chr11	64,509,093	64,513,093	0.42	1.10	2.80	3.43	chr11	64,509,000	64,510,000	-0.50	0.27	-2.52	-1.73	chr11	64,511,629	64,511,630	0.83	-0.81	3.98	4.85	536
RASGRP2	chr11	64,509,093	64,513,093	0.42	1.10	2.80	3.43	chr11	64,509,000	64,510,000	-0.50	0.27	-2.52	-1.73	chr11	64,512,151	64,512,152	0.06	0.32	2.41	2.76	1,058
RASGRP2	chr11	64,509,093	64,513,093	0.42	1.10	2.80	3.43	chr11	64,509,000	64,510,000	-0.50	0.27	-2.52	-1.73	chr11	64,512,328	64,512,329	0.37	1.22	3.02	3.50	1,235
RASGRP2	chr11	64,509,093	64,513,093	0.42	1.10	2.80	3.43	chr11	64,509,000	64,510,000	-0.50	0.27	-2.52	-1.73	chr11	64,512,927	64,512,928	-1.74	-1.62	0.26	0.77	1,834
P4HA3	chr11	74,021,881	74,025,881	-1.03	-0.82	0.48	0.87	chr11	74,022,000	74,023,000	-0.87	0.65	-2.74	-1.81	chr11	74,022,698	74,022,699	0.63	0.38	5.23	6.09	1,183
ZBTB16	chr11	113,929,302	113,933,302	-1.17	-1.20	2.08	2.82	chr11	113,930,000	113,931,000	1.85	1.38	-2.93	-2.68	chr11	113,930,290	113,930,291	-1.74	-1.74	3.05	4.18	1,012
ZBTB16	chr11	113,929,302	113,933,302	-1.17	-1.20	2.08	2.82	chr11	113,930,000	113,931,000	1.85	1.38	-2.93	-2.68	chr11	113,930,431	113,930,432	-1.74	-1.74	0.86	4.68	871
ZBTB16	chr11	113,929,302	113,933,302	-1.17	-1.20	2.08	2.82	chr11	113,931,000	113,932,000	1.30	0.68	-2.10	-4.84	chr11	113,931,288	113,931,289	-1.74	-1.74	3.32	0.23	14
MDM1	chr12	68,725,701	68,729,701	-0.98	-1.36	1.08	1.42	chr12	68,728,000	68,729,000	0.82	0.81	-0.46	-0.95	chr12	68,726,160	68,726,161	1.21	1.33	4.58	5.33	1,541
ATP8A2	chr13	26,035,127	26,039,127	-1.21	-0.96	1.59	1.10	chr13	26,038,000	26,039,000	-0.87	0.98	-2.32	-1.29	chr13	26,037,880	26,037,881	-1.42	-1.74	4.69	3.09	753
RCBTB1	chr13	50,162,794	50,166,794	-1.35	-0.73	0.93	1.48	chr13	50,163,000	50,164,000	-0.49	0.44	-4.08	-1.99	chr13	50,160,506	50,160,507	-1.29	-0.10	1.52	2.75	4,288
PCDH20	chr13	61,986,236	61,990,236	-0.42	-1.31	0.64	0.88	chr13	61,989,000	61,990,000	0.80	0.48	-0.54	-0.80	chr13	61,989,654	61,989,655	-1.74	-1.73	7.59	7.90	1,418
EDNRB	chr13	78,492,207	78,496,207	-1.57	-1.01	0.56	1.77	chr13	78,493,000	78,494,000	-0.08	0.50	-3.34	-2.93	chr13	78,492,965	78,492,966	-1.74	-1.74	6.24	6.21	1,242
EDNRB	chr13	78,491,030	78,495,030	-2.30	-1.20	0.84	1.92	chr13	78,493,000	78,494,000	-0.08	0.50	-3.34	-2.93	chr13	78,493,902	78,493,903	-1.74	-1.74	4.61	4.55	872
CILP	chr15	65,501,240	65,505,240	-1.11	-0.93	1.31	1.51	chr15	65,503,000	65,504,000	1.01	1.63	-1.44	-1.69	chr15	65,503,841	65,503,842	-1.74	-1.74	2.92	3.97	601
XYLT1	chr16	17,562,724	17,566,724	-0.94	-0.30	0.39	0.87	chr16	17,565,000	17,566,000	-0.08	0.89	-2.59	-1.34	chr16	17,564,779	17,564,780	1.48	1.21	3.71	4.47	55
CMIP	chr16	81,689,108	81,693,108	-0.32	-0.61	2.41	1.77	chr16	81,689,000	81,690,000	-0.51	0.33	-2.17	-2.17	chr16	81,684,902	81,684,903	-1.74	-1.74	1.94	2.72	6,206
NECAB2	chr16	84,026,032	84,030,032	-1.52	-0.93	1.15	0.52	chr16	84,027,000	84,028,000	-0.05	0.25	-1.13	-1.56	chr16	84,027,048	84,027,049	-1.74	-1.74	1.46	0.37	984
KIAA0182 NCRNA00311	chr16	85,196,783	85,200,783	-0.69	-1.15	0.90	0.88	chr16	85,200,000	85,201,000	-0.31	0.71	-1.73	-0.53	chr16	85,202,891	85,202,892	3.70	4.04	6.04	6.03	4,108
LOC100506388	chr17	181,628	185,628	-0.96	-0.40	2.49	2.54	chr17	181,000	182,000	0.17	1.24	-2.06	-1.57	chr17	180,937	180,938	-1.74	-1.74	2.20	3.39	2,691
RPH3AL	chr17	233,717	237,717	-1.93	-0.53	0.46	1.20	chr17	235,000	236,000	1.66	0.12	0.18	-2.44	chr17	236,010	236,011	-0.61	-0.47	1.30	0.58	293
CAMKK1	chr17	3,790,520	3,794,520	0.99	-0.25	3.29	2.57	chr17	3,790,000	3,791,000	-0.19	1.33	-2.69	-0.83	chr17	3,794,036	3,794,037	-1.74	-1.74	1.87	0.04	1,516
ALOX15B	chr17	7,942,105	7,946,105	-1.29	-1.57	0.94	1.73	chr17	7,943,000	7,944,000	1.91	2.22	0.90	0.99	chr17	7,942,358	7,942,359	-1.74	-1.74	2.23	3.66	1,747
ALOX15B GUCY2D	chr17	7,942,105	7,946,105	-1.29	-1.57	0.94	1.73	chr17	7,944,000	7,945,000	-0.22	0.58	-2.06	-4.18	chr17	7,944,657	7,944,658	-1.74	-1.74	-0.35	0.17	552
PEMT	chr17	17,482,835	17,486,835	-0.30	-1.55	2.59	1.55	chr17	17,485,000	17,486,000	-0.34	0.54	-2.10	-2.40	chr17	17,485,744	17,485,745	-1.74	-1.74	-0.26	0.74	909
RASL10B	chr17	34,056,814	34,060,814	-0.80	-1.04	0.70	1.47	chr17	34,059,000	34,060,000	-0.29	0.35	-1.70	-1.94	chr17	34,058,679	34,058,680	1.95	1.80	4.58	5.62	135
SPHK1	chr17	74,378,120	74,382,120	2.09	1.08	3.91	2.69	chr17	74,378,000	74,379,000	-0.21	0.73	-1.76	-0.80	chr17	74,378,881	74,378,882	-1.74	-1.19	1.72	1.82	1,239
SPHK1	chr17	74,378,120	74,382,120	2.09	1.08	3.91	2.69	chr17	74,378,000	74,379,000	-0.21	0.73	-1.76	-0.80	chr17	74,380,690	74,380,691	1.82	1.31	6.00	5.70	570
SPHK1	chr17	74,378,120	74,382,120	2.09	1.08	3.91	2.69	chr17	74,378,000	74,379,000	-0.21	0.73	-1.76	-0.80	chr17	74,381,289	74,381,290	-0.17	-1.44	2.95	2.34	1,169
C1QTNF1	chr17	77,014,621	77,018,621	-1.21	-0.86	1.28	0.37	chr17	77,016,000	77,017,000	1.13	0.94	-1.37	-1.07	chr17	77,020,251	77,020,252	3.96	4.10	6.59	6.56	3,630
FASN	chr17	80,058,458	80,062,458	-0.83	-0.66	2.30	2.09	chr17	80,059,000	80,060,000	-0.84	0.38	-2.88	-2.68	chr17	80,056,105	80,056,106	4.64	5.28	7.61	8.34	4,353
EPB41L3	chr18	5,627,045	5,631,045	-0.87	-0.28	0.52	1.80	chr18	5,629,000	5,630,000	0.33	0.05	-2.67	-3.44	chr18	5,630,744	5,630,745	-1.74	-1.37	2.23	4.10	1,699

Table S8A: List of up-regulated promoter regions accompanied with reciprocal changes of H3K27ac and H3K27me3 modifications upon decidualization (125 TSSs of 90 RefSeq genes) (2/2)

Locus	Normalized enrichment scores for H3K27ac window (4,000bp)							Normalized enrichment scores for H3K27me3 window (1,000bp)							FPKM values of the TSS located wihtin 5,000bp from the H3K27ac window								
	Chromosome	Start (hg19)	End (hg19)	EM0409D0_K27ac_log2	EM0519D0_K27ac_log2	EM0409D4_K27ac_log2	EM0519D4_K27ac_log2	Chromosome	Start (hg19)	End (hg19)	EM0409D0_K27me3_log2	EM0519D0_K27me3_log2	EM0409D4_K27me3_log2	EM0519D4_K27me3_log2	Chromosome	Start (hg19)	End (hg19)	EM0409D0_fpkm_log2	EM0519D0_fpkm_log2	EM0409D4_fpkm_log2	EM0519D4_fpkm_log2	Distance of TSS to the center of the H3K27ac window (4,000bp)
APCDD1	chr18	10,452,604	10,456,604	0.41	0.52	1.59	2.59	chr18	10,454,000	10,455,000	-0.12	0.25	-1.16	-2.40	chr18	10,454,554	10,454,555	3.65	3.37	5.62	7.03	50
SERPINB2	chr18	61,557,471	61,561,471	-1.07	-1.02	1.05	1.04	chr18	61,559,000	61,560,000	-0.33	0.30	-2.76	-2.40	chr18	61,554,939	61,554,940	1.83	0.69	6.12	5.02	4,532
RGL3	chr19	11,529,621	11,533,621	-2.33	-0.89	1.39	2.03	chr19	11,530,000	11,531,000	1.22	0.85	-1.45	-1.79	chr19	11,530,018	11,530,019	0.88	1.25	3.32	4.10	1,603
PODNL1	chr19	14,045,707	14,049,707	-0.27	-0.45	1.57	1.33	chr19	14,047,000	14,048,000	1.15	0.71	-0.56	-0.88	chr19	14,049,288	14,049,289	0.92	1.10	4.75	5.14	1,581
PODNL1	chr19	14,045,707	14,049,707	-0.27	-0.45	1.57	1.33	chr19	14,047,000	14,048,000	1.15	0.71	-0.56	-0.88	chr19	14,049,610	14,049,611	-1.64	-1.63	1.86	1.05	1,903
CPAMD8	chr19	17,005,371	17,009,371	-1.17	-0.28	1.15	1.80	chr19	17,007,000	17,008,000	0.91	1.78	-0.19	0.19	chr19	17,007,772	17,007,773	-0.75	-0.30	1.28	2.10	401
FXYD1	chr19	35,628,619	35,632,619	0.59	0.11	2.91	2.43	chr19	35,630,000	35,631,000	-0.49	0.01	-4.13	-4.80	chr19	35,629,732	35,629,733	2.03	0.23	4.00	3.50	887
FXYD1	chr19	35,628,619	35,632,619	0.59	0.11	2.91	2.43	chr19	35,630,000	35,631,000	-0.49	0.01	-4.13	-4.80	chr19	35,630,392	35,630,393	-0.27	-1.74	1.47	2.07	227
FXYD1	chr19	35,628,619	35,632,619	0.59	0.11	2.91	2.43	chr19	35,630,000	35,631,000	-0.49	0.01	-4.13	-4.80	chr19	35,630,501	35,630,502	0.78	-0.08	2.74	2.68	118
DMKN	chr19	36,003,215	36,007,215	-0.82	-0.45	1.29	0.82	chr19	36,005,000	36,006,000	0.41	2.13	-2.15	0.19	chr19	36,004,632	36,004,633	0.84	-0.23	2.03	1.52	583
LYPD3	chr19	43,970,025	43,974,025	-0.42	-0.19	1.65	1.78	chr19	43,970,000	43,971,000	1.54	1.01	0.44	-0.29	chr19	43,969,830	43,969,831	-1.74	-1.64	-0.70	0.62	2,195
PTGIR	chr19	47,126,641	47,130,641	-0.02	-0.50	2.54	0.83	chr19	47,129,000	47,130,000	-0.13	0.06	-1.42	-1.03	chr19	47,128,398	47,128,399	-0.64	-1.59	3.36	2.29	243
GREB1	chr2	11,621,163	11,625,163	-0.76	-0.99	1.73	0.47	chr2	11,623,000	11,624,000	1.60	1.51	0.03	0.24	chr2	11,622,863	11,622,864	-1.74	-1.74	3.89	3.66	300
GREB1	chr2	11,653,698	11,657,698	-1.57	-1.20	1.88	1.25	chr2	11,655,000	11,656,000	0.29	0.86	-2.26	-2.68	chr2	11,655,966	11,655,967	-1.74	-1.74	2.25	2.46	268
GREB1	chr2	11,670,866	11,674,866	-1.03	-1.32	3.52	2.78	chr2	11,674,000	11,675,000	0.41	0.42	-3.66	-2.88	chr2	11,674,242	11,674,243	-1.74	-1.74	4.46	2.76	1,376
GREB1	chr2	11,678,174	11,682,174	-1.57	-0.66	1.68	2.04	chr2	11,680,000	11,681,000	0.38	1.76	-2.32	-0.24	chr2	11,680,080	11,680,081	-1.74	-1.74	1.19	-0.03	94
IL1RL1	chr2	102,919,426	102,923,426	-1.23	-0.71	1.13	1.04	chr2	102,921,000	102,922,000	-0.60	-0.15	-2.63	-2.52	chr2	102,927,962	102,927,963	-1.74	-1.74	1.27	0.57	6,536
TMEM37	chr2	120,182,263	120,186,263	-0.52	-0.47	2.14	1.73	chr2	120,182,000	120,183,000	1.09	0.46	-0.13	-1.23	chr2	120,188,791	120,188,792	-1.74	-1.74	-0.55	-0.04	4,528
TNS1	chr2	218,868,283	218,872,283	-1.69	-0.72	2.62	1.63	chr2	218,870,000	218,871,000	-0.63	0.51	-1.70	-3.92	chr2	218,867,758	218,867,759	4.13	3.44	5.33	5.51	2,525
PNKD	chr2	219,192,787	219,196,787	-1.61	-2.19	0.81	0.50	chr2	219,195,000	219,196,000	-0.03	0.35	-2.11	-2.28	chr2	219,187,902	219,187,903	2.33	2.55	5.27	5.59	6,885
INHA	chr2	220,441,833	220,445,833	-1.27	-0.82	2.77	2.88	chr2	220,442,000	220,443,000	-0.01	0.09	-1.94	-2.08	chr2	220,436,954	220,436,955	-0.25	-0.39	2.94	2.87	6,879
HDAC4	chr2	240,319,509	240,323,509	1.77	0.52	3.61	2.72	chr2	240,319,000	240,320,000	-0.43	0.65	-2.55	-1.24	chr2	240,322,705	240,322,706	3.41	3.36	5.05	5.05	1,196
C20orf27	chr20	3,742,717	3,746,717	-0.11	-0.17	2.08	2.04	chr20	3,744,000	3,745,000	-0.36	0.54	-2.67	-2.06	chr20	3,741,666	3,741,667	3.51	3.66	6.61	6.79	3,051
C20orf27	chr20	3,744,917	3,748,917	-1.34	-0.49	1.43	0.75	chr20	3,744,000	3,745,000	-0.36	0.54	-2.67	-2.06	chr20	3,748,451	3,748,452	-1.21	-0.23	2.52	3.37	1,534
AHCY	chr20	32,891,175	32,895,175	-0.92	-0.66	0.84	0.57	chr20	32,893,000	32,894,000	-0.31	0.13	-2.90	-2.98	chr20	32,891,214	32,891,215	4.45	4.49	5.88	6.43	1,961
TTPAL	chr20	43,098,787	43,102,787	-1.17	-0.82	1.37	1.22	chr20	43,100,000	43,101,000	0.05	0.33	-1.86	-2.17	chr20	43,104,307	43,104,308	0.57	1.31	2.17	3.32	3,520
C21orf63	chr21	33,779,268	33,783,268	-0.98	-0.88	1.02	0.54	chr21	33,780,000	33,781,000	0.17	0.76	-1.30	-0.66	chr21	33,783,161	33,783,162	-0.84	-1.17	2.10	0.90	1,893
C21orf63	chr21	33,780,199	33,784,199	-1.61	-0.35	1.15	1.40	chr21	33,780,000	33,781,000	0.17	0.76	-1.30	-0.66	chr21	33,783,694	33,783,695	0.22	0.54	1.86	2.83	1,495
COL18A1	chr21	46,817,379	46,821,379	-1.27	-1.39	0.49	0.95	chr21	46,821,000	46,822,000	-0.47	0.11	-1.90	-1.16	chr21	46,825,031	46,825,032	4.04	4.08	5.73	7.25	5,652
KIAA1644	chr22	44,701,555	44,705,555	1.12	0.83	2.58	2.40	chr22	44,702,000	44,703,000	0.06	1.62	-1.33	-1.28	chr22	44,708,827	44,708,828	1.21	0.73	3.38	3.00	5,272
KLF15	chr3	126,070,779	126,074,779	-0.51	-0.72	0.99	1.25	chr3	126,071,000	126,072,000	-0.83	0.42	-3.25	-2.32	chr3	126,075,898	126,075,899	0.09	-1.02	1.59	0.36	3,119
LRRC15	chr3	194,094,615	194,098,615	-1.49	-1.18	2.81	2.12	chr3	194,095,000	194,096,000	0.35	0.14	-0.88	-1.39	chr3	194,090,471	194,090,472	-1.74	-1.74	7.48	6.46	6,144
ADRA2C	chr4	3,767,014	3,771,014	1.11	1.59	3.91	4.46	chr4	3,768,000	3,769,000	-0.07	0.05	-3.37	-3.44	chr4	3,768,296	3,768,297	5.23	5.50	8.76	9.32	718
ADRA2C	chr4	3,767,014	3,771,014	1.11	1.59	3.91	4.46	chr4	3,768,000	3,769,000	-0.07	0.05	-3.37	-3.44	chr4	3,768,413	3,768,414	0.69	3.15	5.08	6.84	601
ADRA2C	chr4	3,767,014	3,771,014	1.11	1.59	3.91	4.46	chr4	3,769,000	3,770,000	1.96	1.57	-2.32	-3.51	chr4	3,768,615	3,768,616	-1.74	-1.74	1.29	1.28	399
SLC10A6	chr4	87,767,552	87,771,552	-0.91	-0.58	2.21	2.27	chr4	87,771,000	87,772,000	0.99	0.71	-1.22	-0.74	chr4	87,770,415	87,770,416	-1.74	-1.74	2.64	2.12	863
SLC10A6	chr4	87,767,552	87,771,552	-0.91	-0.58	2.21	2.27	chr4	87,771,000	87,772,000	0.99	0.71	-1.22	-0.74	chr4	87,770,565	87,770,566	-1.74	-1.74	0.89	0.66	1,013
SETD7	chr4	140,478,549	140,482,549	-1.17	-0.61	2.03	1.67	chr4	140,479,000	140,480,000	0.53	0.62	-1.99	-2.48	chr4	140,477,576	140,477,577	5.11	4.73	6.28	6.23	2,973
LOC100506688	chr5	996,525	1,000,525	-0.53	-0.76	3.22	3.04	chr5	998,000	999,000	1.57	1.22	-0.03	-1.70	chr5	997,505	997,506	-1.74	-1.74	0.70	1.51	1,020
CHSY3	chr5	130,219,879	130,223,879	-0.89	-2.04	0.85	1.11	chr5	130,220,000	130,221,000	0.47	0.31	-2.65	-3.13	chr5	130,220,573	130,220,574	-1.74	-1.74	1.52	0.00	1,306
ADAMTS2	chr5	178,769,652	178,773,652	2.80	1.87	4.21	3.38	chr5	178,773,000	178,774,000	0.49	1.24	-0.95	-0.62	chr5	178,772,430	178,772,431	5.66	5.44	7.78	8.26	778
ADAMTS2	chr5	178,769,652	178,773,652	2.80	1.87	4.21	3.38	chr5	178,773,000	178,774,000	0.49	1.24	-0.95	-0.62	chr5	178,772,536	178,772,537	4.19	4.94	6.19	7.62	884
CNR1	chr6	88,874,149	88,878,149	-0.75	-0.88	1.85	2.50	chr6	88,876,000	88,877,000	2.62	2.85	-0.45	0.59	chr6	88,875,766	88,875,767	-1.74	-1.74	6.75	6.43	383
CNR1	chr6	88,874,149	88,878,149	-0.75	-0.88	1.85	2.50	chr6	88,876,000	88,877,000	2.62	2.85	-0.45	0.59	chr6	88,876,311	88,876,312	-1.74	-1.74	5.98	6.41	162
CNR1	chr6	88,874,149	88,878,149	-0.75	-0.88	1.85	2.50	chr6	88,876,000	88,877,000	2.62	2.85	-0.45	0.59	chr6	88,876,511	88,876,512	-1.74	-1.74	3.18	3.90	362
LOC441177	chr6	166,400,334	166,404,334	-0.46	-0.57	2.38	2.42	chr6	166,400,000	166,401,000	2.22	1.14	-4.08	-3.34	chr6	166,401,039	166,401,040	-1.74	-1.71	2.64	3.79	1,295
C6orf176	chr6	166,398,661	166,402,661	-1.06	-1.10	3.28	3.51	chr6	166,402,000	166,403,000	2.18	1.80	-2.99	-3.05	chr6	166,401,526	166,401,527	-1.71	-0.80	3.87	4.00	865
HDAC9	chr7	18,125,503	18,129,503	-1.14	-1.04	0.41	1.65	chr7	18,127,000	18,128,000	0.35	0.85	-1.39	-1.90	chr7	18,126,572	18,126,573	-1.74	-1.74	1.32	2.49	931
HDAC9	chr7	18,125,503	18,129,503	-1.14	-1.04	0.41	1.65	chr7	18,127,000	18,128,000	0.35	0.85	-1.39	-1.90	chr7	18,126,877	18,126,878	-1.74	-1.74	-0.55	1.96	626
ADCY1	chr7	45,747,365	45,751,365	-0.13	-0.08	3.99	4.23	chr7	45,749,000	45,750,000	-0.51	0.81	-3.74	-4.29	chr7	45,749,697	45,749,698	-1.74	-1.74	0.85	0.61	332
ABCB8	chr7	150,726,973	150,730,973	-0.54	-1.33	3.06	2.52	chr7	150,730,000	150,731,000	-0.46	0.42	-2.69	-2.17	chr7	150,725,510	150,725,511	2.62	2.75	4.30	4.39	3,463
SCARA5	chr8	27,848,719	27,852,719	-0.80	-1.23	0.81	1.01	chr8	27,851,000	27,852,000	0.37	0.95	-1.27	-0.46	chr8	27,849,752	27,849,753	-1.74	-1.74	4.98	4.96	967
SCARA5	chr8	27,848,719	27,852,719	-0.80	-1.23	0.81	1.01	chr8	27,851,000	27,852,000	0.37	0.95	-1.27	-0.46	chr8	27,850,368	27,850,369	-1.74	-1.74	6.48	6.30	351
DNAI1	chr9	34,510,518	34,514,518	-1.19	-1.24	3.30	2.75	chr9	34,513,000	34,514,000	0.64	1.26	-2.32	-0.44	chr9	34,513,796	34,513,797	-1.74	-1.74	2.19	1.88	1,278
TMC1	chr9	75,419,248	75,423,248	-1.57	-1.29	1.54	1.59	chr9	75,421,000	75,422,000	0.87	0.90	-0.27	-0.70	chr9	75,423,647	75,423,648	-1.74	-1.74	0.48	0.94	2,399
PCSK5	chr9	78,505,829	78,509,829	-0.90	-0.19	1.06	1.20	chr9	78,509,000	78,510,000	0.00	-0.13	-1.99	-2.40	chr9	78,505,554	78,505,555	2.68	3.49	4.84	5.62	2,275
GADD45G	chr9	92,216,998	92,220,998	-0.56	-1.14	2.80	1.31	chr9	92,218,000	92,219,000	0.82	-0.21	-2.41	-1.28	chr9	92,219,927	92,219,928	1.25	0.75	7.60	6.75	929
ROR2	chr9	94,711,791	94,715,791	-1.43	-1.05	0.85	0.34	chr9	94,711,000	94,712,000	2.43	1.21	-3.15	-1.99	chr9	94,712,443	94,712,444	2.03	2.16	4.85	4.59	1,348
ROR2	chr9	94,709,651	94,713,651	-0.10	-0.15	2.31	1.32	chr9	94,713,000	94,714,000	0.21	0.12	-1.93	-1.73	chr9	94,713,126	94,713,127	-0.91	-0.37	1.65	2.36	1,475
COL15A1	chr9	101,806,653	101,810,653	-1.03	-1.21	2.35	2.86	chr9	101,808,000	101,809,000	1.14	0.74	-0.82	-1.94	chr9	101,809,447	101,809,448	-1.74	-1.74	-0.03	1.17	794
SLC46A2	chr9	115,653,174	115,657,174	-1.86	-0.88	0.58	0.49	chr9	115,653,000	115,654,000	2.05	1.68	-0.15	0.40	chr9	115,653,251	115,653,252	-1.74	-1.74	3.50	2.49	1,923
LAMC3	chr9	133,885,900	133,889,900	-0.07	-0.95	3.86	2.93	chr9	133,887,000	133,888,000	0.91	0.87	-1.50	-0.65	chr9	133,884,504	133,884,505	1.76	1.43	5.79	5.59	3,396

Table S8B: List of down-regulated promoter regions accompanied with reciprocal changes of H3K27ac and H3K27me3 modifications upon decidualization (45 TSSs of 38 RefSeq genes)

Locus	Normalized enrichment scores for H3K27ac window (4,000bp)							Normalized enrichment scores for H3K27me3 window (1,000bp)							FPKM values of the TSS located wihtin 5,000bp from the H3K27ac window							
	Chormosome	Start (hg19)	End (hg19)	EM0409D0_K27ac_log2	EM0519D0_K27ac_log2	EM0409D4_K27ac_log2	EM0519D4_K27ac_log2	Chormosome	Start (hg19)	End (hg19)	EM0409D0_K27me3_log2	EM0519D0_K27me3_log2	EM0409D4_K27me3_log2	EM0519D4_K27me3_log2	Chormosome	Start (hg19)	End (hg19)	EM0409D0_fpkm_log2	EM0519D0_fpkm_log2	EM0409D4_fpkm_log2	EM0519D4_fpkm_log2	Distance of TSS to the center of the H3K27ac window (4,000bp)
COL16A1	chr1	32,166,460	32,170,460	0.64	1.84	-1.11	-0.34	chr1	32,169,000	32,170,000	-3.63	-2.61	0.02	-1.16	chr1	32,169,767	32,169,768	3.89	4.73	0.28	1.17	1,307
COL16A1	chr1	32,166,460	32,170,460	0.64	1.84	-1.11	-0.34	chr1	32,169,000	32,170,000	-3.63	-2.61	0.02	-1.16	chr1	32,169,978	32,169,979	2.61	3.57	-1.74	-1.53	1,518
CRABP2	chr1	156,675,283	156,679,283	1.73	1.76	-1.07	-1.59	chr1	156,676,000	156,677,000	-2.08	-2.25	-0.56	-0.24	chr1	156,675,458	156,675,459	3.49	4.74	-1.54	-0.98	1,825
PEAR1	chr1	156,870,232	156,874,232	2.08	1.82	-1.26	-0.80	chr1	156,872,000	156,873,000	-4.01	-1.59	-1.13	-0.57	chr1	156,874,733	156,874,734	0.79	0.89	-1.25	-1.74	2,501
PRELP	chr1	203,442,416	203,446,416	0.87	0.81	-0.91	-1.16	chr1	203,444,000	203,445,000	-3.41	-3.49	-0.64	-0.95	chr1	203,444,883	203,444,884	3.56	4.52	-1.74	-0.43	467
CAMK1D	chr10	12,389,671	12,393,671	2.06	2.31	0.29	0.28	chr10	12,390,000	12,391,000	-3.41	-2.70	-1.34	-1.40	chr10	12,391,508	12,391,509	3.97	4.42	1.62	1.79	163
FRMD4A	chr10	13,749,001	13,753,001	0.57	1.16	-1.15	-1.00	chr10	13,750,000	13,751,000	-2.53	-2.10	-1.34	-0.39	chr10	13,749,877	13,749,878	0.98	0.99	-0.57	-0.70	1,124
CXCL12	chr10	44,877,943	44,881,943	1.27	2.01	-1.28	-1.17	chr10	44,879,000	44,880,000	-1.07	-1.38	0.67	-0.05	chr10	44,880,544	44,880,545	5.42	6.14	2.12	3.13	601
LOXL4	chr10	100,026,943	100,030,943	1.48	1.29	-0.32	-1.06	chr10	100,029,000	100,030,000	-2.67	-1.11	-0.81	0.24	chr10	100,028,029	100,028,030	4.50	4.88	2.11	2.13	914
ADRA2A	chr10	112,835,219	112,839,219	3.26	3.48	-1.51	-1.16	chr10	112,835,000	112,836,000	0.68	-0.66	2.53	1.00	chr10	112,836,790	112,836,791	7.09	7.29	-0.43	0.69	429
BDNF	chr11	27,718,345	27,722,345	0.42	1.26	-1.02	-0.99	chr11	27,721,000	27,722,000	-1.51	-2.28	-0.30	-0.56	chr11	27,722,034	27,722,035	1.69	1.61	-1.60	-0.94	1,689
MRGPRF	chr11	68,780,428	68,784,428	1.28	1.96	-0.58	-0.79	chr11	68,781,000	68,782,000	-3.57	-2.67	-2.08	-0.84	chr11	68,780,849	68,780,850	4.91	5.43	0.46	1.35	1,579
PTHLH	chr12	28,120,716	28,124,716	3.03	3.57	-0.73	0.23	chr12	28,122,000	28,123,000	-2.88	-3.49	-1.39	-1.66	chr12	28,122,893	28,122,894	2.64	2.63	-1.74	-1.74	177
NDUFA4L2	chr12	57,631,795	57,635,795	0.29	1.89	-0.87	-1.97	chr12	57,635,000	57,636,000	0.80	0.96	2.10	2.11	chr12	57,634,474	57,634,475	0.85	1.33	-1.74	-1.63	679
ARHGEF40	chr14	21,537,147	21,541,147	2.58	2.75	1.46	1.10	chr14	21,537,000	21,538,000	-2.84	-2.45	-1.17	-0.74	chr14	21,537,859	21,537,860	0.12	1.04	-1.02	-0.96	1,288
NPAS3	chr14	33,406,545	33,410,545	2.61	2.31	1.45	0.77	chr14	33,407,000	33,408,000	0.19	-0.29	1.62	1.41	chr14	33,407,927	33,407,928	-0.20	0.52	-1.43	-0.80	618
TGFB3	chr14	76,446,400	76,450,400	2.34	2.28	0.00	0.13	chr14	76,446,000	76,447,000	-1.51	-0.97	0.06	0.26	chr14	76,448,091	76,448,092	3.53	3.64	-0.29	-1.74	309
TGFB3	chr14	76,446,400	76,450,400	2.34	2.28	0.00	0.13	chr14	76,446,000	76,447,000	-1.51	-0.97	0.06	0.26	chr14	76,449,314	76,449,315	0.56	1.09	-1.74	-1.14	914
ZNF469	chr16	88,447,826	88,451,826	1.50	2.50	-1.32	-1.74	chr16	88,450,000	88,451,000	-1.89	-3.10	-0.32	-1.45	chr16	88,449,196	88,449,197	1.66	3.19	-1.64	-1.26	630
CCL2	chr17	32,574,258	32,578,258	0.73	0.72	-1.10	-1.48	chr17	32,578,000	32,579,000	-0.60	-0.77	0.80	0.36	chr17	32,582,296	32,582,297	0.21	2.06	-1.74	-0.53	6,038
TYMS	chr18	656,019	660,019	0.39	0.74	-1.37	-0.93	chr18	657,000	658,000	-1.12	-1.18	0.07	-0.15	chr18	657,604	657,605	2.93	3.29	-1.74	-1.74	415
C18orf56	chr18	656,019	660,019	0.39	0.74	-1.37	-0.93	chr18	657,000	658,000	-1.12	-1.18	0.07	-0.15	chr18	658,339	658,340	-0.53	-0.54	-1.74	-1.74	320
NEDD4L	chr18	55,709,440	55,713,440	0.86	1.18	-0.91	-1.65	chr18	55,712,000	55,713,000	-1.05	-1.04	0.61	0.32	chr18	55,711,619	55,711,620	0.92	0.82	-1.65	-1.08	179
CYS1	chr2	10,217,865	10,221,865	3.00	2.98	1.10	0.34	chr2	10,220,000	10,221,000	0.19	-2.65	1.55	-0.66	chr2	10,220,537	10,220,538	2.99	3.26	1.34	1.73	672
LBH	chr2	30,447,044	30,451,044	2.62	2.25	-0.85	-1.32	chr2	30,451,000	30,452,000	-1.83	-1.75	-0.11	-0.41	chr2	30,454,397	30,454,398	7.98	8.22	5.40	5.37	5,353
LRP1B	chr2	142,886,629	142,890,629	1.43	1.42	0.06	-0.01	chr2	142,888,000	142,889,000	-2.27	-2.52	-1.27	-1.32	chr2	142,889,269	142,889,270	1.08	0.59	-0.29	-1.22	640
JAG1	chr20	10,651,015	10,655,015	0.58	1.29	-1.25	-1.71	chr20	10,655,000	10,656,000	-2.57	-1.86	-1.47	-0.70	chr20	10,654,693	10,654,694	1.84	2.07	0.51	-0.27	1,678
PDGFB	chr22	39,637,415	39,641,415	3.15	3.28	0.18	-0.93	chr22	39,640,000	39,641,000	-2.02	-3.37	-0.13	-1.00	chr22	39,637,862	39,637,863	-0.51	-0.24	-1.74	-1.74	1,553
PDGFB	chr22	39,637,415	39,641,415	3.15	3.28	0.18	-0.93	chr22	39,640,000	39,641,000	-2.02	-3.37	-0.13	-1.00	chr22	39,640,956	39,640,957	3.49	4.10	0.69	1.11	1,541
GXYLT2	chr3	72,937,762	72,941,762	0.83	0.78	-1.17	-1.40	chr3	72,937,000	72,938,000	-0.13	-2.61	1.28	-0.69	chr3	72,937,385	72,937,386	1.50	1.79	-1.74	-1.26	2,377
B3GALNT1	chr3	160,820,627	160,824,627	0.99	1.19	-1.05	-1.43	chr3	160,822,000	160,823,000	-1.12	-1.94	-0.01	0.03	chr3	160,822,682	160,822,683	1.14	-0.11	-1.74	-1.74	55
B3GALNT1	chr3	160,820,627	160,824,627	0.99	1.19	-1.05	-1.43	chr3	160,822,000	160,823,000	-1.12	-1.94	-0.01	0.03	chr3	160,823,159	160,823,160	2.01	1.80	-0.44	-0.79	532
CLDN11	chr3	170,134,276	170,138,276	0.50	0.72	-1.12	-1.95	chr3	170,137,000	170,138,000	-0.56	-0.99	0.50	0.65	chr3	170,136,653	170,136,654	4.30	4.50	0.48	-0.55	377
EDIL3	chr5	83,677,362	83,681,362	2.06	1.77	0.02	-0.68	chr5	83,679,000	83,680,000	-3.34	-1.47	-1.76	-0.24	chr5	83,680,610	83,680,611	3.59	3.26	2.24	2.12	1,248
EDIL3	chr5	83,677,362	83,681,362	2.06	1.77	0.02	-0.68	chr5	83,679,000	83,680,000	-3.34	-1.47	-1.76	-0.24	chr5	83,680,736	83,680,737	4.20	3.75	2.79	2.09	1,374
SYNPO	chr5	150,019,587	150,023,587	2.50	2.65	0.75	0.60	chr5	150,019,000	150,020,000	-1.73	-1.77	-0.40	0.23	chr5	150,020,176	150,020,177	3.77	4.10	-0.09	-0.01	1,411
ADRA1B	chr5	159,341,479	159,345,479	1.24	1.85	-1.31	0.04	chr5	159,345,000	159,346,000	-1.87	-2.04	-0.60	-0.87	chr5	159,343,382	159,343,383	2.25	2.59	-1.74	-0.68	97
ADRA1B	chr5	159,341,479	159,345,479	1.24	1.85	-1.31	0.04	chr5	159,345,000	159,346,000	-1.87	-2.04	-0.60	-0.87	chr5	159,343,740	159,343,741	3.99	3.92	-0.68	0.36	261
STC2	chr5	172,752,492	172,756,492	2.67	2.94	0.98	-0.75	chr5	172,756,000	172,757,000	-2.53	-1.93	-0.58	-0.38	chr5	172,754,438	172,754,439	4.16	2.95	2.16	0.14	54
TNXB	chr6	32,074,978	32,078,978	2.95	2.86	0.21	0.07	chr6	32,077,000	32,078,000	-3.84	-1.94	-2.06	-0.14	chr6	32,077,150	32,077,151	7.64	7.69	4.24	4.36	172
WNT2	chr7	116,961,006	116,965,006	4.37	4.66	-0.12	-0.39	chr7	116,962,000	116,963,000	-1.05	-1.58	1.64	-0.12	chr7	116,962,315	116,962,316	3.72	3.03	-1.04	-1.74	691
WNT2	chr7	116,961,006	116,965,006	4.37	4.66	-0.12	-0.39	chr7	116,962,000	116,963,000	-1.05	-1.58	1.64	-0.12	chr7	116,963,342	116,963,343	6.56	6.48	1.91	1.44	336
PSAT1	chr9	80,909,618	80,913,618	0.65	2.29	-1.20	-0.61	chr9	80,911,000	80,912,000	-2.16	-3.49	-1.13	-0.06	chr9	80,912,059	80,912,060	5.22	5.76	1.76	1.64	441
OLFML2A	chr9	127,539,411	127,543,411	2.10	1.86	0.58	-0.46	chr9	127,542,000	127,543,000	-1.61	-1.36	-0.09	-0.30	chr9	127,539,437	127,539,438	5.34	4.79	3.15	1.75	1,974
ANGPTL2	chr9	129,882,748	129,886,748	2.46	2.64	0.83	-0.13	chr9	129,885,000	129,886,000	-3.68	-2.10	-1.51	0.36	chr9	129,885,099	129,885,100	5.98	5.98	3.72	2.80	351

Table S9: The extents of gene activation and repression upon decidualization for the gene sets with reciprocal changes of H3K27ac and H3K27me3 at their promoter region and for the gene sets with H3K27ac change only.

Donor	FPKM log2 median FPKM log2 fold-change (fc) median	Up-regulated genes		Down-regulated genes	
		H3K27ac-up only	H3K27ac-up H3K27me3-down	H3K27ac-down only	H3K27ac-down H3K27me3-up
		664 genes	306 genes	816 genes	220 genes
EM0409	FPKM log2 (D0)	0.63	-0.08	1.83	2.49
	FPKM log2 (D4)	1.91	2.24	0.60	0.86
	FPKM log2 (D8)	2.04	2.31	0.42	0.40
	FPKM log2 fc (D4 vs D0)	0.83	1.66	-0.77	-0.97
	FPKM log2 fc (D8 vs D0)	0.84	1.60	-0.89	-1.35
EM0519	FPKM log2 (D0)	0.70	-0.36	1.86	2.37
	FPKM log2 (D4)	1.94	2.25	0.63	0.74
	FPKM log2 (D8)	2.13	2.59	0.46	0.44
	FPKM log2 fc (D4 vs D0)	0.83	1.64	-0.59	-0.91
	FPKM log2 fc (D8 vs D0)	1.05	1.68	-0.68	-1.14
average	FPKM log2 (D0)	0.67	-0.22	1.84	2.43
	FPKM log2 (D4)	1.92	2.24	0.61	0.80
	FPKM log2 (D8)	2.09	2.45	0.44	0.42
	FPKM log2 fc (D4 vs D0)	0.83	1.65	-0.68	-0.94
	FPKM log2 fc (D8 vs D0)	0.95	1.64	-0.79	-1.25